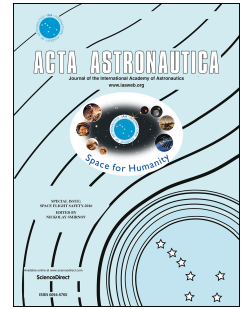


# Journal Pre-proof

Space Environment Considerations for Perovskite Solar Cell Operations: A Review

Meghan Bush, Jeremiah Sims, Samuel S. Erickson, Kaitlyn VanSant, Sayantani Ghosh, Joseph M. Luther, Lyndsey McMillon-Brown



PII: S0094-5765(25)00307-8

DOI: <https://doi.org/10.1016/j.actaastro.2025.05.025>

Reference: AA 11163

To appear in: *Acta Astronautica*

Received Date: 26 August 2024

Revised Date: 7 May 2025

Accepted Date: 15 May 2025

Please cite this article as: M. Bush, J. Sims, S.S. Erickson, K. VanSant, S. Ghosh, J.M. Luther, L. McMillon-Brown, Space Environment Considerations for Perovskite Solar Cell Operations: A Review, *Acta Astronautica*, <https://doi.org/10.1016/j.actaastro.2025.05.025>.

This is a PDF file of an article that has undergone enhancements after acceptance, such as the addition of a cover page and metadata, and formatting for readability, but it is not yet the definitive version of record. This version will undergo additional copyediting, typesetting and review before it is published in its final form, but we are providing this version to give early visibility of the article. Please note that, during the production process, errors may be discovered which could affect the content, and all legal disclaimers that apply to the journal pertain.

© 2025 Published by Elsevier Ltd on behalf of IAA.



# Space Environment Considerations for Perovskite Solar Cell Operations: A Review

Meghan Bush<sup>1</sup>, Jeremiah Sims<sup>1</sup>, Samuel S. Erickson<sup>2</sup>, Kaitlyn VanSant<sup>1,3</sup>, Sayantani Ghosh<sup>2</sup>, Joseph M. Luther<sup>3</sup>, and Lyndsey McMillon-Brown<sup>1</sup>

<sup>1</sup>Photovoltaic and Electrochemical Systems Branch, NASA Glenn Research Center, Cleveland, Ohio, USA

<sup>2</sup>Department of Physics, University of California, Merced, California, USA

<sup>3</sup>National Renewable Energy Laboratory, Golden, CO, USA

## Corresponding Author

\*E-mail: [lyndsey.mcmillon-brown@nasa.gov](mailto:lyndsey.mcmillon-brown@nasa.gov)

Tel: 1 216-433-5197

## Author Contributions

The manuscript was written through contributions of all authors. All authors have given approval to the final version of the manuscript.

## Abstract

Designing new technology for extraterrestrial applications certainly presents unique challenges. The environmental stressors perovskites must overcome will vary with the environment in which they are deployed. One must consider mission requirements when designing photovoltaic devices and packaging. Different space “theaters” can have dramatically different stressors needing consideration for designing panels for solar power generation. In this article, we review the relevant space environmental conditions that must be considered when designing perovskite-based photovoltaic devices for implementation in space. We specifically consider thermal, radiation, gaseous, weather, and other phenomena most relevant to photovoltaic operation for specific theaters such as Low Earth Orbit, Geosynchronous Orbit, Lunar surface, Mars (orbit and surface), and interplanetary exploration pathways.

**Keywords:** solar cell, durability, perovskite solar cell, photovoltaic, space, lunar, mars, deep space, low earth orbit, geosynchronous orbit, space environments, spacecraft charging

## Acronyms:

AM0	air mass zero
AM1.5G	air mass 1.5 global
AU	astronomical unit
CME	coronal mass ejections
CTE	coefficient of thermal expansion
EQE	external quantum efficiency
FF	fill factor
GEO	geosynchronous equatorial orbit
GCR	galactic cosmic rays
LEO	low Earth orbit
LILT	low intensity, low temperature
LIHT	low intensity, high temperature
MISSE	Materials International Space Station Experiment
NOAA	National Oceanic and Atmospheric Administration
PCE	power conversion efficiency
PV	photovoltaic
RTG	radioisotope thermoelectric generator
SCR	solar cosmic rays
SEP	solar energetic particles
UV	ultraviolet

## 1. Introduction

Perovskite-based photovoltaics show great promise for integration into space. Recent advancements demonstrate radiation tolerance and resilience to thermal and vacuum stress [1], [2], [3]. Initial long duration flight in low Earth orbit (LEO) verifies viability for this technology to perform in space [4]. Perovskite-based photovoltaics are a promising candidate to support extended human space presence, meeting the need for very large (>100 kW) and high-voltage-capable solar arrays. Perovskites can be designed with materials selection and barrier layers to overcome environmental stressors [5]. There is a breadth of work on strategies to improve the perovskite device performance [6], [7], [8], [9], [10], conduct reliable measurements [11], and achieve commercial deployment [12], [13], [14], largely with considerations for terrestrial applications. For the reader interested in recent advancements of perovskite photovoltaic device design, we recommend the following reviews [14], [15], [16], [17]. Other reviews have evaluated the prospects for perovskite-based photovoltaics in space and have discussed the technological challenges and potential advantages [18], [19], [20], [21]. Specifically, previous work has detailed perovskite photovoltaic light instability, thermal cycling stress response, and vacuum stress challenges, while highlighting device resilience to high energy radiation exposure, light weight, flexibility, and the potential for commercial scale up. These reviews largely focus on LEO and lunar applications or approach space as a homogenous environment. However, the environmental stressors perovskites must overcome will vary with the environment in which they are deployed. One must consider mission requirements when designing photovoltaic devices and packaging. Here, we assess low Earth orbit (LEO), geosynchronous orbit (GEO), lunar, Martian, and interplanetary space environments and discuss the space environmental conditions relevant to perovskite-based photovoltaics. These specific environments were selected for their current and emerging opportunities for perovskite photovoltaic (PV) operation.

The implementation of photovoltaic arrays in LEO is rapidly increasing as proliferated LEO (pLEO) materializes and hundreds of thousands of satellites are deployed and linked to one another creating networks for global internet constellations and various applications [19]. LEO describes the region of space with an altitude at or below 2000 km (1242 mi) above the Earth's surface; it is a popular destination for satellites and is home to the International Space Station (ISS). Objects in LEO are exposed to a myriad of hazards including vacuum pressures of  $10^{-10}$  torr, ultraviolet (UV) radiation, thermal fluctuations, space radiation, and atomic oxygen [22].

Geosynchronous Equatorial Orbit (GEO), also known as Geostationary Orbit, is an orbit sitting at about 35,786 km (22,236 mi) above the equator. Objects in GEO have an orbital period equal to Earth's rotational period (23 hours and 56 minutes) or in synchronous patterns to Earth's rotational period. GEO is of interest for space based solar power beaming installations to convert incident solar power to electricity that is then beamed to earth at radio frequency to a rectenna. The requirement for very large (multiple km across) arrays with high performance and reliability at competitive costs makes worthwhile to consider if perovskites may contribute to this application. GEO is an environment with high levels of ionizing radiation and an extremely high vacuum level (around  $10^{-14}$  torr) [22]. When exposed to a vacuum level this high, the main concern for PV devices is the release of absorbed substances in the form of gas from the material it is trapped in, also known as outgassing.

The Moon and Mars are the primary focus for the National Aeronautics Space Administration's (NASA) Artemis program. Developing a thorough understanding of the Moon has been a goal of NASA since the beginnings of the agency. The Artemis program aims to establish a human presence on the surface of the

Moon. Artemis missions will build upon the legacy of space photovoltaics by utilizing solar power for lunar missions. Perovskites are an attractive option for lunar surface power due to their low mass, potential flexibility, tunable bandgap, high efficiency, and low cost (\$/W) [1], [23]. However, they must be able to survive the Moon's extreme and variable environment. In addition to the design of perovskites for long duration operation on the Moon, there is also interest in manufacturing these devices on the lunar surface [23]. Like the Moon, the operation of solar cells on Mars presents unique challenges. For many Mars missions, the performance of the photovoltaic array is a driving operational constraint on the permissible latitude of the landing site, the amount of power available for science instruments, and how long scientific operations can operate each day [24]. In addition to government space programs, there is interest from private enterprise to enable colonization of both the Moon and Mars.

We do not discuss Mercury and Venus in this review since currently the viability for perovskite solar cell deployment in these environments is low. Mercury has very high solar intensity yielding daytime temperatures (430 °C) too extreme for perovskite-based photovoltaic operation. In addition to being our hottest planet, Venus is continually covered in sulfuric acid clouds which obscure the sun, resulting in low irradiance at the surface. The hostile Venusian environment is not suitable for current perovskite photovoltaic technology, and although previous research has been done on low-intensity high-temperature (LIHT) solar cells that could survive at Venus [25], [26], [27], this has not yet included perovskites.

Solar power has successfully been used to power spacecraft on numerous NASA missions, although it has yet to be deployed at distances beyond Jupiter, approximately 5.5 astronomical units (AU). To-date, spacecraft missions beyond Jupiter have been powered by radioisotope thermoelectric generators (RTGs). The interplanetary space power environment is described as low intensity and low temperature (LILT). Irradiance decreases quadratically with distance from the Sun, requiring a larger solar array surface area for photovoltaic-powered exploration of deep space destinations. Interplanetary space missions present new opportunities for perovskite solar cells in LILT environments. Other environmental challenges in these regions include charged particles and atmospheric effects. Perovskites hold potential for performance in missions to outer planetary systems which necessitate high specific power and low-cost deployable systems.

The development of perovskite-based photovoltaics for space applications affords new opportunities while presenting unique technical challenges. Perovskite-based photovoltaic devices being designed for any of the abovementioned environments must be optimized optically for the air-mass zero (AM0) solar spectrum to increase absorption and decrease reflection. Devices must be resilient to UV radiation, which has higher intensities at AM0 compared to the terrestrial air mass 1.5 global (AM 1.5G) solar spectrum. Perovskite-based photovoltaics are well suited to this task since their microstructures can be manipulated at the nanoscale to improve optoelectronic characteristics, stability, and overall performance. Perovskite adopts an  $ABX_3$  crystal structure, where the A-site is generally filled with either an organic molecule like methylammonium ( $CH_3NH_3^+$  or MA), formamidinium ( $NH_2CHNH_2^+$  or FA), or a Cs inorganic cation. The B-site is typically a metal cation like  $Pb^{2+}$ ,  $Sn^{2+}$ , or another divalent metal cation. The X represents a halide ion like  $Cl^-$ ,  $Br^-$ , or  $I^-$ . By adjusting chemical composition, perovskites can be tuned to span bandgaps ranging from 1.1 eV ( $MASnI_3$ ) to 3.1 eV ( $MAPbCl_3$ ). By varying the cation ratio (e.g. replacing some or all of the MA with FA) and adjusting the mixed metal and/or halide compounds (e.g.  $MAPbI_xBr_{3-x}$ ), one can achieve bandgaps in-between [28], [29], [30], [31], [32]. The microstructure of perovskite which includes crystal orientation, morphology, and grain size, are major factors in light harvesting capability, decreased recombination losses, and enhanced charge [33], [34]. Perovskite devices can be designed to achieve high power conversion efficiency, increased operational stability, and resilience against

environmental stressors encountered in space. Further, the low mass of perovskite PV is ideal for integration in space where high specific power (>30 Watt/kg) is a necessity [35]. There is also a desire to realize very large (>100 kW) and high-voltage-capable (300-600 V) solar array systems. Presently, a suitable long duration high voltage power supply system does not exist. The following sections of this paper provide a thorough review of the environmental factors that will impact perovskite-based photovoltaic performance and durability. The subsections report the relevant conditions (thermal, radiation, vacuum, atomic oxygen, and other natural phenomena) for each respective location (LEO, GEO, lunar, Mars and interplanetary) as it pertains to the environmental conditions that are most relevant to photovoltaic operation.

## 2. Solar Irradiance and the Thermal Environment

Perovskite-based photovoltaics are sensitive to thermal cycling and operating at extreme temperatures which are largely induced by the intensity of incident sunlight and waste heat of the energy conversion process. Thermal cycling often induces microcracking of substrates or coatings and/or delamination of coatings. Microcracking can serve as a pathway for atomic oxygen ingress and bombardment of underlying material. Thermal cycling also poses a threat to materials with shared interface but substantially different coefficient of thermal expansion. This can lead to coating delamination from substrate or stresses in the coating(s), either of which can greatly diminish or terminate the performance of a solar cell. These phenomena have been observed in the first long-duration LEO flights of perovskite active layer on the Materials International Space Station Experiment (MISSE) platform [4].

It is a general rule that photovoltaic output decreases as temperature increases. This is largely due to the temperature dependence of the bandgap ( $E_g$ ) of traditional semiconductors shown in the Varshni relation **Equation 1** [36]. Here,  $E_g(T)$  is the bandgap of the semiconductor at temperature  $T$ ,  $E_g(0)$  is the bandgap at 0 K, and  $\alpha$  and  $\beta$  are material dependent constants. The decrease in the bandgap with increasing temperature results in a slight increase in short-circuit current and an impactful decrease in the open-circuit voltage. This behavior is opposite in perovskites, and is well understood [37], [38], and relates to the band inversion symmetry (s-like valence and double degenerate p-like conduction bands) in perovskite materials [39]. In general, the energy gap increases with increasing perovskite operating temperature [37].

$$E_g(T) = E_g(0) - \frac{\alpha T^2}{(T + \beta)} \quad \text{Equation 1}$$

The ultimate performance of a solar cell is determined by PV parameters including open-circuit voltage ( $V_{oc}$ ), short-circuit current ( $J_{sc}$ ), fill factor (FF), and power conversion efficiency (PCE), all of which are temperature dependent. Generally, the  $J_{sc}$  increases with increasing temperature, and the associated  $V_{oc}$  decrease is from the defect concentration which can be attributed to the high recombination rate with increasing temperature. The low FF at low temperatures is due to increased charge carrier diffusion resistance [37]. An increase in temperature over the room temperature generally decreases the perovskite solar cell efficiency. At low temperature ( $T < 120$  K), the charge transport layer limits the device performance, while at high temperature ( $T > 200$  K), the interfacial charge recombination becomes the dominant factor [40]. In **Figure 1** we summarize the temperature extremes and solar irradiances of relevant regions and planetary bodies within our solar system, adapted from reference [41]. Perovskite-based photovoltaics can suffer from thermal instability when exposed to the Sun; the cell temperature can be up

to 45°C higher than ambient environmental temperature in terrestrial operation [42]. The target temperature for operation of perovskite-based solar cells in lunar and LEO applications is 75°C [5], [43]. A perovskite solar cell retained 92% of its power conversion efficiency after stress testing at 85°C and 85% relative humidity according to international standard (IEC 61215) for just 1000 hours [44]. The elevated temperatures can cause the decomposition of perovskite into  $\text{PbI}_2$  and the device performance rapidly degrades at operating temperatures greater than 150°C [45]. At finite temperatures, organic-inorganic Pb halide perovskites may exhibit three perovskite phases: the cubic ( $\alpha$ ), tetragonal ( $\beta$ ), and orthorhombic ( $\gamma$ ) phases [39]. The bandgap increases from the cubic phase (ideal perovskite) to the tetragonal and orthorhombic phases (distorted perovskites) for Pb halide perovskites [39], [46], [47], [48]. At temperatures greater than 100°C, an intermediate phase of the perovskite absorber between the tetragonal and cubic phase begins to emerge and the device loses performance [49], [50]. We should note, a perovskite active layer flown on MISSE for 10 months showed significantly suppressed transition temperature from tetragonal to orthorhombic by nearly 65 K when compared to ground-based control, subsequently broadening the photovoltaic operational range [4]. Residual strain in the film caused by rapid thermal cycling (4800 cycles in 10 months) has been identified as the most significant factor in altering the transition temperature allowing the tetragonal phase to stabilize thermodynamically. The thermal stability of perovskite absorber materials has been improved by engineering the perovskite composition. Recent development of perovskite solar cell for operation in space revealed that engineering of the contact layer and barrier layers has significant impact on the device performance when exposed to heat (75°C) and vacuum stress. Researchers successfully demonstrated a perovskite-based photovoltaic device stable under thermal-vacuum stress for more than 3500 hours [3]. Despite these known sensitivities to elevated temperatures, a proper heat treatment time can passivate defects, resulting in a 15% relative improvement of average efficiency for perovskite-based photovoltaics [45]. At low temperatures, perovskite-based photovoltaics operate well. However, a noticeable reduction of the external quantum efficiency (EQE) is evident below 600 nm in the solar spectrum [38].

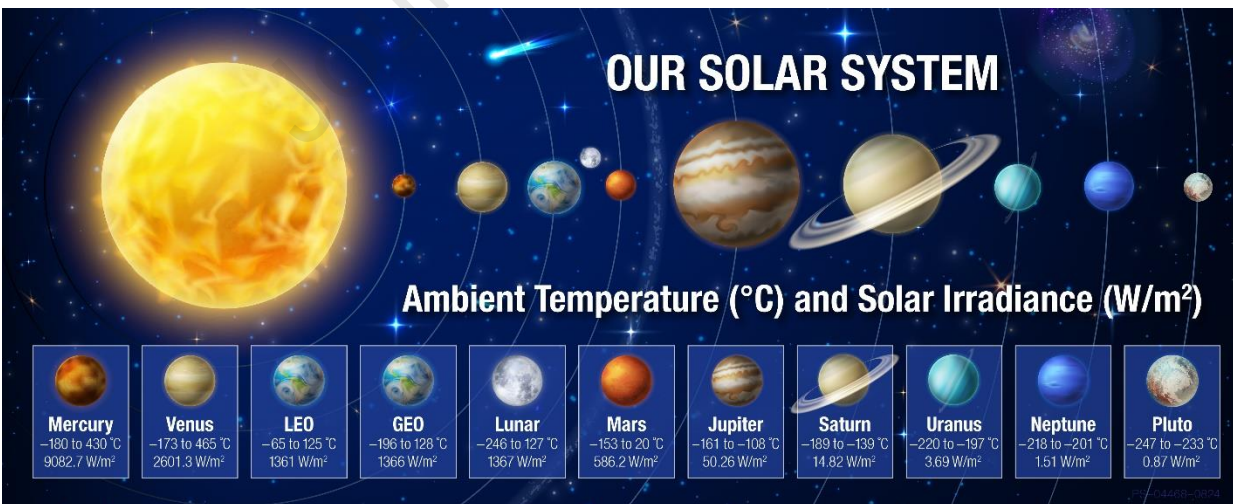


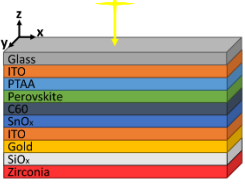
**Figure 1.** Ambient temperature range (°C) and corresponding solar irradiance (W/m<sup>2</sup>) for planetary bodies and orbits of interest in our solar system.

## 2.1. Low Earth Orbit (LEO)

LEO has three primary sources of radiant thermal energy: incoming solar radiation, earth reflected solar energy (albedo) and outgoing longwave radiation emitted by the Earth and its atmosphere [51]. Albedo, the solar energy reflected from the planet and its atmosphere is highly variable across the globe and is dependent on both the distribution of reflective properties of the surface and the amount and type of cloud cover. Reflectivity increases with increased cloud cover [51].

While in LEO, a spacecraft orbits Earth approximately every 90 minutes, or 6000 times a year. Each orbit consists of a heating phase in the sunlight followed by a cooling period in Earth's shadow. Solar panels in LEO can reach 100°C while heated by the Sun's radiation and -80°C during eclipse as the panel radiates to cold space. The thermal cycles create a considerable temperature fluctuation that induces thermal stresses on the system components. The amplitude of the temperature cycle depends on the material properties such as emittance, absorptance, thermal conductivity, and specific heat [52]. UV radiation reaching an intensity of 118 W/m<sup>2</sup> is seen with ranging from 2220-5800 equivalent Sun hours per year (ESH/yr) [22]. The absence of a UV absorber, like ozone, in LEO means extreme levels of UV radiation are reaching the photovoltaics and increasing the device temperature. When selecting perovskite-based photovoltaics for missions in LEO, one should seek materials with a similar coefficient of thermal expansion (CTE). This, coupled with careful selection of a backside material and a maximal electrical power conversion efficiency, can aid in managing the operating temperature of the perovskite. A triple-cation perovskite active layer, however, is predicted to endure more than 460 years of thermal cycling in LEO before it undergoes thermal induced mechanical failure [5], suggesting that research focus should target other constituent layers (e.g. transport layers, electrodes) to extend device lifetime. This computation modeled the cell as a plate with spatially uniform temperature assuming constant properties for specific heat and density, and negligible incident radiation on the sides. The ambient temperature and light illumination were simulated, and the transient heat equation was solved for a perovskite-based photovoltaic in LEO. The expected number of thermal cycles to mechanical failure for materials in a perovskite-based photovoltaic are shown in **Table 1**. Generally, perovskite-based photovoltaics have similar material properties (density, specific heat, bandgap) therefore these results can provide insight to most device architectures.

**Table 1.** Number of thermal cycles to mechanical failure for each of the components of the solar cell stack. Adapted from ref [5]. Inset image of the modeled photovoltaic device layers.

	Material	Cycles to failure	Years to failure in LEO
	Zirconia	45,628	8.07
	Glass	$4.468 \times 10^{12}$	$7.898 \times 10^8$
	Triple Cation	$2.604 \times 10^6$	460.4
	SiO <sub>x</sub>	$2.234 \times 10^{11}$	$3.949 \times 10^7$

## 2.2. Geosynchronous Equatorial Orbit (GEO)

With little ozone absorbing the spectral irradiance from the Sun, solar irradiance in GEO is roughly 1366 W/m<sup>2</sup> at 1 AU. Solar duration is constant until the autumn and spring equinox, where spacecrafts are shadowed by the Earth for 70 minutes a day over 2 periods of 45 days [22]. At altitudes above 20 km from the Earth's surface, albedo and IR become less of an environmental load on space systems and solar irradiation becomes the most significant load. The UV spectrum contains ~99% of the total energy of all electromagnetic radiation coming from the Sun. The intensity of UV radiation increases at higher levels of vacuum. In GEO, an intensity of 118 W/m<sup>2</sup> is seen with about 8760 equivalent Sun hours per year (ESH/yr)

[22]. Temperature conditions are similar to LEO, except colder temperatures are experienced when the spacecraft enters the Earth's shadow. This period, known as eclipse season, occurs twice a year (around the spring and autumn equinox) over a period of 45 days, for 70 minutes each day. Therefore, temperature cycling in GEO conditions is  $-196^{\circ}\text{C}$  to  $128^{\circ}\text{C}$ , 90 cycles/year [22].

### 2.3. Lunar

The temperature on the Moon varies with location and the lunar day-night cycle [53]. At the equator, the lunar day-night cycle is approximately 29.5 Earth days, consisting of 14.75 days of constant sunlight followed by 14.75 days of darkness due to the Moon's synchronous rotation with Earth. Additionally, the illumination profile varies greatly with the latitude and local topography of the Moon [54]. Under illumination, the surface can reach up to  $\sim 397\text{ K}$  ( $123.85^{\circ}\text{C}$ ) at the equator and  $\sim 200\text{ K}$  ( $-73.15^{\circ}\text{C}$ ) at the poles, which drops to roughly  $95\text{ K}$  ( $-178.15^{\circ}\text{C}$ ) and  $50\text{ K}$  ( $-223.15^{\circ}\text{C}$ ) respectively during the lunar night. Permanently shadowed regions can reach temperatures as low as  $33\text{ K}$  ( $-240^{\circ}\text{C}$ ). Solar cells and all array materials must be robust enough to withstand these temperature extremes and cycling throughout the 28 day-night cycle.

Thermal analysis of photovoltaics operating on the lunar surface determined the temperature range of interest is  $-25$  to  $75^{\circ}\text{C}$ , assuming thermal management will prevent the cells from reaching the temperature extremes of the lunar surface environment. This analysis assumed that the photovoltaic array was thermally isolated from its lander and Sun-pointing throughout the transit. A high-pressure fiberglass laminate, G10, was used for thermal isolation [43]. Recent studies into the design of a perovskite-based photovoltaic for lunar applications focused on the combination of contact and barrier layers to maximize device stability under thermal vacuum stress. VanSant et al. revealed that indium tin oxide (ITO) and Au contacted cells with barrier layers consisting of  $\text{SiO}_x$  and both  $\text{SiO}_x$  and a space-qualified silicone encapsulant (DC 93-500) and cover glass assembly retained more than 90% of their performance after 3600 hours of vacuum-thermal stress. When the devices were exposed to a combination of light, heat, and high vacuum, the ITO-contacted cells demonstrated superior stability and are thus the recommended contacting scheme for a perovskite-based photovoltaic for lunar applications [3].

### 2.4. Mars

The operating temperature of a solar cell will impact cell efficiency, and performance. When considering what will impact the cell temperature on a planetary surface both radiation losses and wind convection must be considered. An expression that depends upon the ambient temperature ( $T_a$ ), solar irradiance ( $\phi_s$ ), and wind speed ( $u$ ) is introduced in reference [55] and shown in **Equation 2**. This analysis assumed the Mars atmosphere was 100%  $\text{CO}_2$ , with density ( $\rho = 0.01308\text{ kg/m}^3$ ), kinematic viscosity ( $\nu = 0.0010868\text{ m}^2/\text{s}$ ), dust opacity index ( $\gamma = 0.3$ ), and forced convection under Mars conditions. The average surface temperature on Mars is  $-65^{\circ}\text{C}$ . Due to its thin atmosphere, Mars loses heat rapidly. The ambient temperature can range from  $20^{\circ}\text{C}$  to  $-153^{\circ}\text{C}$  [56]. Temperature sensors on Opportunity reported an average high of  $13.8^{\circ}\text{C}$  and average low of  $-100^{\circ}\text{C}$  [57]. Equation 2 is expected to hold for the case of perovskite photovoltaics. Perovskite-based photovoltaic cells for Mars should be designed to endure temperatures spanning from  $-100^{\circ}\text{C}$  to  $20^{\circ}\text{C}$  for operation near the equator. This is considered low temperature operation for photovoltaics. The lower temperature, coupled with the redder spectrum, tend to better suit lower bandgap solar cell technologies [24].

$$T_c = 1.00116 \cdot T_a + 0.0313174 \cdot \phi_s - 0.108832 \cdot u \quad \text{Equation 2}$$

## 2.5. Interplanetary Space

In the LILT environment, lower irradiance leads to a reduction in solar cell efficiency. Lowering the operating temperature can improve cell efficiency, but extremely low temperatures can lead to cell degradation. Jupiter is 5.1 AU away from the Sun, resulting in a solar irradiance that is only 3.7% of AM0 [58]. The expected operating temperature of a solar cell at Jupiter is expected to be within -125 and -140°C [59]. Saturn (9.5 AU) has an irradiance of 1.1% AM0 with an expected solar cell operating temperature of -165°C [58], [59]. Saturn mission concept designs often include a gravity assist maneuver that would involve a near-Venus trajectory [60], meaning that even though the solar cells will already need to be able to operate in extreme LILT conditions, they may also need to withstand solar array temperatures up to 150°C near Venus [61]. The performance of solar cells in Saturn-relevant conditions has been studied using ground-based LILT testing and compared to solar cells used on the Juno mission, which was launched in 2011 to investigate Jupiter. When Juno was inserted into Jupiter's orbit in 2016, its solar arrays briefly experienced temperature and high-angle irradiance conditions that emulated a Saturn-like environment. This provided an opportunity to compare ground-based solar cell test results under LILT conditions to in-flight performance, independently validating ground test data [59].

Triple-cation perovskite device performance has been investigated under conditions consistent with those found in Jupiter and Saturn orbits [62]. The current-voltage response of devices under conditions consistent with LILT show no significant degradations, with  $V_{OC}$  and  $J_{SC}$  reductions commensurate with the reduced intensity without additional thermally mediated parasitic losses or other nonradiative processes. In LILT conditions, the current-voltage response is hysteresis-free, which is consistent with the “freezing-out” of ionic motion [63]. The observed electrical performance confirms the potential for stable performance of these systems in LILT. Variable temperature external quantum efficiency (EQE, 80 to 300K) and variable temperature photoluminescence (PL, 4 to 280 K) are anticorrelated, meaning that with decreasing temperature, EQE decreases while PL intensity increases. It is believed that a combination of the ionization of the exciton binding energy (at higher temperatures) in the perovskite and an unintentional barrier for minority electron extraction becomes more prevalent at low temperature and higher intensity, yielding the observed optoelectronic performance. It is notable that the absorber maintained its cubic structure between 4.2 and 300 K. There were no observed low-temperature phase inclusions, alloy fluctuations, nor any indication of structural phase change. These findings suggest that a formamidinium, methylammonium, and cesium containing perovskite system offers a stable system in interplanetary space.

At Uranus (19.2 AU, 0.28% AM0 irradiance) and Neptune (30 AU, 0.1% AM0 irradiance), operating temperatures are expected to be -224°C and -245°C respectively [58], [64]. The extreme LILT environment of these so-called “Ice Giants” would require significant solar cell and array technology improvements beyond the current state of practice before photovoltaics could be considered a viable power source [58]. Perovskite photovoltaics operating under these conditions have yet to be reported in the literature.

## 2.6. Summary

In this section we summarize the solar irradiance and thermal environments of various locations where perovskite-based photovoltaic devices may be deployed in space. The most challenging thermal

environments will likely be orbital theatres with rapid thermal cycling. Ideally, coefficients of thermal expansion between layers should be minimized in photovoltaic device design. Further study into depositing and/or annealing perovskite absorber layers at temperatures closer to their operational range is one pathway to reduce residual stress in the material during the mission. Additional ground-based testing should be conducted to explore the impact of extended low-temperature operation of perovskite-based photovoltaics under illumination, simulating lunar, Mars, and LILT mission profiles.

### 3. Ionizing Radiation and Plasma

Radiation in space consists of a wide spectrum of particles that lose energy when transmitting through matter. The radiation can be ionizing (high energy) or non-ionizing (low energy). Ionizing radiation causes inelastic ionizing energy loss (IEL), which results in localized heating due to scattering with the surrounding electron cloud. Non-ionizing radiation results in non-ionizing energy loss (NIEL), which displaces atoms and creates vacancies within the lattice structure. Radiation in space is generated by particles emitted from a variety of sources both within and beyond our solar system. The three major sources of charged-particle radiation in free space are galactic cosmic rays (GCR), trapped radiation belts, and solar energetic particle events [65]. Examples of ionizing radiation include alpha particles, beta particles, gamma rays, x-rays, and GCR. GCR originate from beyond our solar system (up to 100 AU from the Sun) and contain particles of all charges from protons to uranium nuclei with energies from MeV to  $10^{15}$  MeV/nucleon. The particle flux of GCR is observed to vary by about 15% across the solar cycle [66]. GCR is lowest during solar maximum and highest during solar minimum. At solar maximum, the Sun's magnetic field is stronger, and it deflects more GCR particles, reducing the GCR flux at Earth [67]. Solar flares release many electrons, protons, x-rays, and gamma rays with kinetic energies ranging from keV to GeV [68]. Trapped radiation belts contain mostly protons and electrons; deuterons and tritons contribute less than 1% of the total proton flux. The properties of the resulting defects play critical roles in the resulting device performance. Point defects with energy levels deep in the bandgap act as Shockley-Read-Hall nonradiative recombination centers, which are primarily responsible for short minority carrier lifetime and thus a low  $V_{oc}$  [39].

Existing American Institute of Aeronautics and Astronautics (AIAA) S-111 standards mandate that solar cells withstand  $1e13$  fluence at 3 MeV protons per square cm ( $p^+/cm^2$ ) and  $1e16$  fluence at 1 MeV electrons per square cm ( $e^-/cm^2$ ) [69]. These standards have been determined for conventional (III-V and Silicon) solar cells, but radiation-matter interactions in perovskite-based photovoltaics are different from conventional photovoltaics. As such, the AIAA S-111 standards are being revisited as the community conducts investigations to determine equivalent fluences to achieve similar damage [1], [2], [70], [71], [72], [73], [74]. To date, experiments have been conducted to determine the tolerance of perovskite solar cells under electron [70], [75], proton [2], [70], [71], [72], [73], [74], [76], [77], [78], [79], [80], neutron [81], and  $\gamma$ -ray irradiations [82], [83], [84]. It should be noted that to appropriately evaluate device performance quartz substrates should be employed instead of soda-lime glass, because soda-lime glass becomes darkened by radiation. This substrate degradation may otherwise impact the evaluation of radiation tolerance of the devices, falsely yielding reduced  $J_{sc}$ .

Low-energy protons (0.05-0.15 MeV) create a representative uniform damage profile, whereas higher energy protons necessitate much higher fluence to achieve the equivalent displacement damage dose due to a lower scattering probability [1]. Further, it has been observed that high-energy protons (1.0 MeV) effectively anneal radiation damage caused by lower-energy protons (0.6 MeV) and recover device efficiency. This is due to the phonon vibrations (caused by the IEL) that drive the displaced atoms back to

lattice positions, suppressing the non-radiative recombination and increasing device PCE [2]. Simulated annual proton fluences for key orbits of interest are shown in **Figure 2A**.

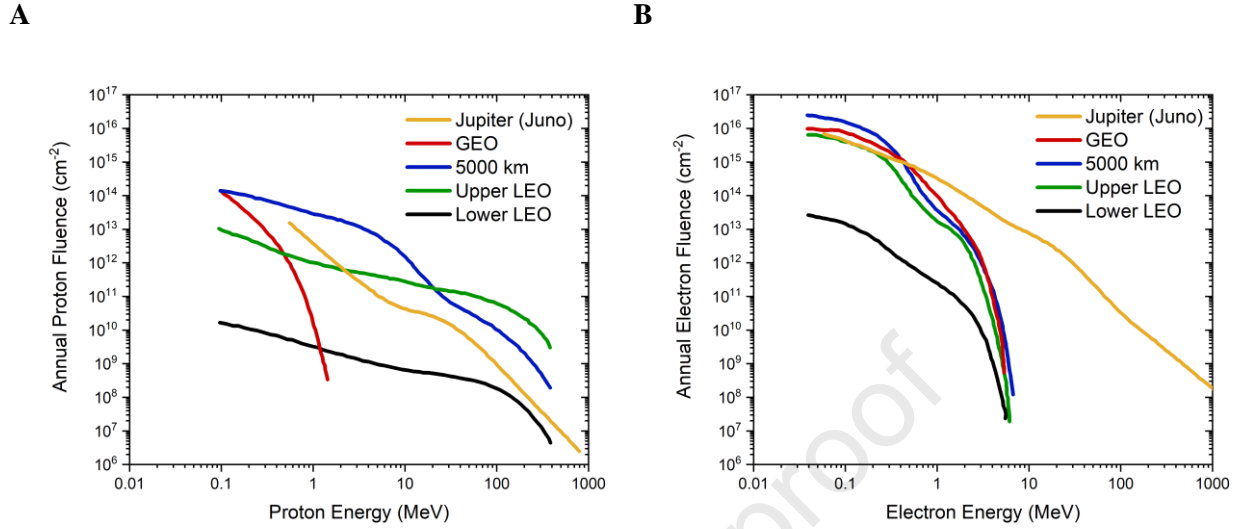


**Figure 2.** Simulated annual fluences from the Space Environment Information System (SPENVIS) as a function of **A)** proton energy and **B)** electron energy for lower-LEO (ISS 420 km) (black), upper-LEO (2000 km) (green), 5,000 km (blue), GEO (red), and Jupiter (Juno) orbits (yellow); adapted from ref [1]

Note: A and B show integral fluences; visit <https://spenvis.oma.be/> for differential spectra.

Electrons are among the most common high energy particles in space. Annual electron fluences for key orbits of interest are shown in **Figure 2B**. The defects created by electron radiation become minority-carrier recombination centers or majority carrier trap centers. AIAA S-111 standards for electron radiation necessitate that cells withstand  $1e16$  fluence at 1 MeV electrons per square cm ( $e^-/cm^2$ ) [69]. It is noted that the electron radiation shall be conducted at room temperature with beam currents sufficiently low to prevent significant sample heating. Like proton radiation standards, these standards have been determined for conventional (III-V and Silicon) solar cells and should be reconsidered for their equivalent damage dosages for perovskite-based photovoltaics. Miyazawa et al. irradiated cells with 1 MeV  $e^-$  at fluences up to  $1e16$   $e^-/cm^2$  and reported no deterioration in short-circuit current, open-circuit voltage, or external quantum efficiency [70]. Perovskite absorber layers under  $10^{-5}$  torr vacuum were irradiated by 1 MeV electrons from  $1e12$  to  $1e16$   $e^-/cm^2$  with no significant changes in morphology or perovskite crystal phase observed. Device exposure to  $1e16$   $e^-/cm^2$  fluence did yield a 10% degradation in power conversion efficiency; Monte Carlo simulation confirmed that the electrons passed through the perovskite but were stopped in the substrate [75]. Perovskite-based photovoltaics continue to show resilience to electrons as both methylammonium and formamidinium-based lead iodide perovskite solar cells maintained averages  $> 95\%$  of their initial value when irradiated by  $1e16$   $e^-/cm^2$  at 1 MeV [70].

Solar cells are also susceptible to the impacts of spacecraft charging. Impinging electrons cause spacecraft components, including solar cells, to build up an electric charge. Primary arcs occur within a solar cell as the potential difference between the coverglass and the rest of the solar cell components causes a rapid electrostatic discharge into the local environment. Under the right conditions, this can create a highly

energized local plasma field that couples cells on neighboring strings and causes a secondary arc [85], [86]. Secondary arcs are fed by the photogenerated current and will not dissipate on their own. These high-heat events pyrolyze cell components, often fatally destroying cells, and can then deposit contaminants on neighboring cells, resulting in a potentially widespread damage area. Arcing is very dependent on the materials, architecture, and power levels of an array, so care must be taken in the design process [85], [87]. Many resources exist for the design of arrays to minimize arcing [88], [89] and testing of arrays to understand arcing behavior of a given array design [90], [91]. For arrays of perovskite solar cells, both types of arcing are a concern. For multijunction and silicon solar cells, primary arcs are not considered to be an issue, but for thin film solar cells like perovskites, the heat generated during an arcing event may induce thermal stress in the cell and cause significant damage due to the lack of mass to dissipate the heat.

### **3.1. Low Earth Orbit (LEO)**

Radiation in LEO consists of a both non-ionizing and ionizing radiation that lose energy when transmitting through matter and induce NIEL and IEL losses, respectively. The environment is dominated by a dense low-energy plasma. The LEO plasma environment and its interactions with spacecraft have been extensively studied via ground research [92], [93] and using spacecraft like the ISS [94], [95], [96].

Arrays must be designed to withstand the spacecraft charging and arcing environment found in LEO. Mitigation techniques have been identified and widely accepted in the community as design rules to prevent arcing of the resulting photovoltaic array. It is recommended to use string voltages less than 55 V where possible. We have not observed trigger arcs on LEO arrays below this threshold, even under simulated micrometeoroid bombardment [10]. If an array string exceeds 75 V, trigger arcs can be prevented by encapsulating the cell, so they do not interact with ambient plasma. Encapsulation may prevent arcing up to 1000 V string voltage. In instances when encapsulation is not possible, a bakeout of the array on-orbit for 1 week at 100°C or more can eliminate contaminants and prevent the initiation of trigger arcs up to 300 V [10], [11]. The above ideas are best practices to prevent arcing in arrays deployed in LEO. However, each new solar array implementation should be ground-tested in a simulated LEO plasma before one can be certain it will not arc. The bias voltage tested should include the maximum when arrays come out of eclipse. Similarly, the sample temperature should be as low as the eclipse-egress temperature. The inter-string voltage that is tested should be at least equivalent to that expected anywhere on the array on-orbit. If trigger arcs are prevented, sustained arcs cannot occur.

When considering radiation impacts of perovskite solar cells, it is helpful to consider mission-specific variables that will alter the radiation environment. The altitude of the spacecraft above the earth; at higher altitudes the Earth's magnetic field is weaker resulting in less protection against ionizing particles. At higher altitudes, spacecraft pass through the trapped radiation belts more often. Towards the end of the 11-year cycle, during solar maximum, the number and intensity of solar flares significantly increases. Mission-specific design modifications like encapsulation, coverglass thickness, light intensity, and device temperature can be made to increase the viability and performance of perovskite photovoltaics in LEO radiation environments.

### **3.2. Geosynchronous Equatorial Orbit (GEO)**

The Earth's trapped radiation belts are formed by energetic electrons and protons trapped in the Earth's quasi-dipolar magnetic field. GEO orbit is within the outer radiation belt. The radiation environment, when compared to LEO, consists of more energetic electrons and protons at a lower density. It mainly consists of

energetic electrons (1-10 MeV) outside the magnetosphere being pushed into the outer radiation belt by solar winds, protons from solar proton events, and GCR.

GEO is largely occupied by weather monitoring satellites, specifically GOES (Geostationary Operation Environmental Satellites), that monitor Earth's weather and space environments. Data from these satellites are used to create various radiation belt models (AE-9/AP-9) in combination with the European Space Agency's SPENVIS (SPace ENVironment Information System). These models allow for the estimation and prediction of the radiation environment for any specified mission profile. For example, a geostationary orbit single segment mission with a 15-year mission duration generates radiation models for trapped proton and electron fluxes, solar proton fluence spectra, heavy ion fluence spectra, and GCR fluxes [97]. **Figure 3** shows an example plot of the trapped electron spectra for the 15-year mission profile.

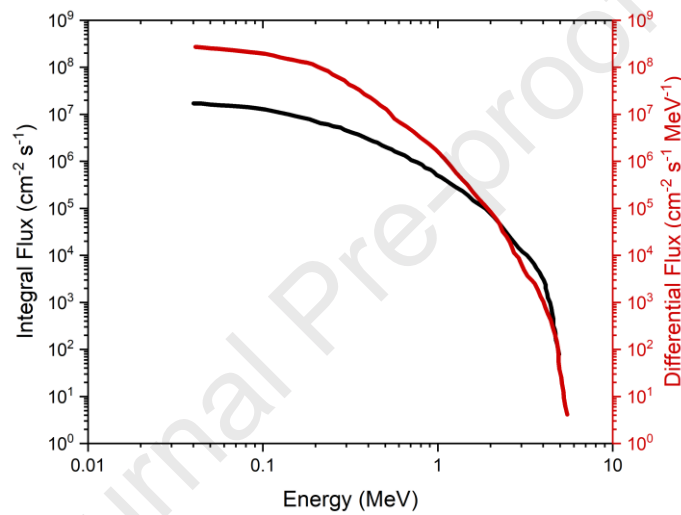


**Figure 3.** Trapped electron spectra created in SPENVIS for a 15-year geostationary orbit mission at AE-8 MAX orbit averaged flux.

The plasma environment in GEO correlates to the radiation environment, which is low in density but high in energy. High energy electrons are hitting spacecraft surfaces at thousands of electron volts, causing the spacecraft itself to charge to potentials of thousands of volts. This builds up a differential voltage between the cell and cover glass, enabling primary and thus secondary arcs [85], [98].

Environmental testing at relevant fluences and energy levels is recommended to determine the performance of perovskite-based photovoltaics in the GEO radiation environment. It will also be critical to investigate the arcing and charging of perovskite-based photovoltaics.

### 3.3. Lunar

The Moon is exposed to solar wind, a plasma consisting of electrons and ions originating from the Sun. This plasma causes charging of regolith, the loose layer of rock and dust covering the lunar surface. The regolith is also excited by incoming UV radiation from sunlight, causing photoemission of electrons [99], [100]. During the lunar day, the surface is positively charged as photoemission dominates. During the lunar night, the surface is negatively charged due to incident electrons [99], [101].

Charging can also have negative impacts on perovskite-based solar arrays through the induction of primary and secondary arcs. The worst-case scenario for spacecraft charging on the lunar surface is similar to GEO as the Moon passes through Earth's geotail; the radiation environment is low in density but consists of very high energy particles [85], [101]. Arcing under GEO is electron-driven and will be highly damaging without proper protection mechanisms [85]. In addition to charging, solar cells will also be exposed to radiation through solar wind (large flux, low energy), galactic cosmic rays (small flux, high energy), and solar cosmic rays (high flux, high energy, result of solar flares) [101]. Particle energies tend to be around 1 eV-5 keV for solar wind [100], 0.1-several GeV for GCR [102], [103], and 1-100 MeV for solar cosmic rays (SCR) [102]. The proton fluxes of each are  $3e8$  protons/cm<sup>2</sup>·s for solar wind, 2-4 protons/cm<sup>2</sup>·s for GCR, and 0-106 protons/cm<sup>2</sup>·s for SCR [101]. On Earth, the magnetosphere and atmosphere protect the surface from these harmful particles through scattering and absorption; however, the Moon has no magnetosphere and extremely little atmosphere [104]. Radiation reaching the Moon primarily consists high energy protons and electrons with some helium and heavy nuclei [101]. Additionally, interactions with the lunar regolith result in the generation of secondary neutrons and gamma rays. Radiation energy is highly dependent on location and the lunar cycle; depending on orbital position and rotation, the Moon will either be primarily exposed to GCR or solar wind [100], [101], [103].

### 3.4. Mars

With no global magnetic field to deflect energetic charged particles, and little atmosphere (<1% that of Earth) to provide shielding, Mars' surface is exposed to radiation. At the surface, the atmosphere provides the equivalent of roughly 20 g/cm<sup>2</sup> of shielding from radiation, and thus radiation is not a significant source of degradation for photovoltaics [24]. The thin atmosphere is not sufficient to stop a large fraction of GCR [105]. GCR are somewhat reduced in passing through the atmosphere but interactions between incoming ions and the atmosphere result in pion production that contributes to exposure on the surface [106]. GCR ions and the Martian soil have nuclear collisions which create an ambient field of neutrons which also contribute to the radiation exposure on the surface. Solar particle events (SPE) are greatly attenuated as they pass through the atmosphere, reduced by an order of magnitude [106]. Mission specific tests of perovskite-based photovoltaics should be completed per specific cell chemistry and array architecture to determine device performance and durability for operation on Mars.

### 3.5. Interplanetary Space

All the outer planets (Jupiter, Saturn, Uranus, Neptune) have a region of space known as the magnetosphere that is strongly influenced by the planet's magnetic field. Charged particles are trapped and accelerated to high energies within the planet's magnetosphere, creating complex radiation dynamics that can damage solar arrays. Jupiter's magnetosphere, the most powerful in the solar system, is particularly vast, covering an area ranging from 3.2 million kilometers towards the Sun and 965.6 million kilometers away from the Sun, extending out to Saturn's orbit [107]. It has a magnetic surface field magnitude approximately 20 times stronger and a dipole moment ~20,000 times that of Earth [108]. Volcanic eruptions on Jupiter's moon Io eject large amounts of sulfur dioxide gas into Jupiter's magnetosphere, forming a torus of plasma that rotates with the planet. This sulfur dioxide is dissociated into atoms and ionized by electron impacts, resulting in sulfur and oxygen ions of varying charge states [109]. These particles interact with the particles associated with Jupiter's faint planetary ring system and may be influenced by high-energy protons from the solar wind, although the extent of the solar wind's effect on the Jovian magnetosphere is not well understood [109], [110]. Estimates of end-of-mission radiation doses vary depending on the orbit; estimates

of recent missions are summarized in **Table 2**. Contours for electron and proton fluxes for the outer planets can be found in reference [111].

The radiation environment at Saturn is significantly less aggressive than that of Jupiter. Saturn also has a magnetosphere, but the extensive particle rings around Saturn tend to deplete the radiation in proximity to regions where calculations predict peak radiation would occur [60]. Based on the assessment of cell efficiencies under Saturn-relevant LILT conditions and the 1.1% AM0 irradiance, a solar-powered Saturn mission would require an array with approximately 10 m<sup>2</sup> active area, or 40 kW of maximum operational capability at 1 AU [59].

**Table 2:** Estimates of end-of-mission interplanetary radiation doses.

	Jupiter	Europa	Saturn	Uranus	Neptune
Radiation	Poles: 7e14, 1MeV e <sup>-</sup> /cm <sup>2</sup>	5e15	2e14	p <sup>+</sup> , e <sup>-</sup> , H <sup>2+</sup>	p <sup>+</sup> , e <sup>-</sup>
Conditions	Equator: 4e15, 1MeV e <sup>-</sup> /cm <sup>2</sup>	1 MeV e <sup>-</sup> /cm <sup>2</sup>	1 MeV e <sup>-</sup> /cm <sup>2</sup>		

According to NASA's 2017 "Solar Power Technologies for Future Planetary Science Missions", the solar power system requirements for outer planetary missions will require solar cells with >38% efficiency under LILT conditions and radiation tolerance up to 6e15, 1 MeV e<sup>-</sup>/cm<sup>2</sup>, particularly for operation in the Jovian environment. The solar array requirements will need to achieve at least 20kW at 1 AU with a lifetime of >15 years, with mass and volume targets that are three times lower than the current SOP of existing solar technologies [58]. The low mass of perovskite-based photovoltaics and their promising performance in LILT conditions suggest they may be suitable to reach the solar array requirements.

### 3.6. Summary

In this section, we summarize the space radiation environment found in the areas of interest for perovskite-based solar power. The risk radiation presents to solar cells is twofold: firstly, particles can induce damage in the cells through IEL (localized heating) and NIEL (displacing atoms in lattice and creating defects). Secondly, charged particles will cause solar cell components to charge and discharge in ESD events known as arcing. These arcs can pyrolyze metal contacts and severely damage the perovskite layer. Representative ground testing is strongly recommended to understand the impacts of environment-specific radiation dosage on solar cells (reference AIAA S111/S112) and arcing rate of a given solar array architecture (reference standard ISO 11221). Though perovskites have shown some resilience to the radiation environment and self-healing capabilities, these tests should be completed per specific cell chemistry and array architecture.

## 4. Vacuum

The primary concern for perovskite solar cells under vacuum is the outgassing of solar cell materials. The main consequences of outgassing are the contamination of surfaces, loss of dimensional stability, and detrimental effects on the material properties [112]. All known surface pressures (weight of the atmosphere per unit area) of planetary bodies within our solar system are reported, in atmospheres, in **Table 3**. LEO vacuum is typically 10<sup>-9</sup> to 10<sup>-11</sup> torr. Perovskite active layers are structurally soft materials. Many organic materials in a vacuum environment will evaporate and molecules adsorbed onto the surface will desorb. Compounds within the material can also diffuse to the material surface and desorb. Organic gas components were released from CH<sub>3</sub>NH<sub>3</sub>PbI<sub>3</sub> (MAPbI<sub>3</sub>) powder [113] and CH(NH<sub>2</sub>)<sub>2</sub>PbI<sub>3</sub> (FAPbI<sub>3</sub>) powder [114] at 10<sup>-7</sup> torr. This decomposition occurred both under light and dark conditions and among the liberated species

were I<sub>2</sub>, HI, NH<sub>3</sub>, CH<sub>3</sub>I, and CH<sub>3</sub>NH<sub>2</sub> from MAPbI<sub>3</sub>, and HI, HCN, and NH<sub>3</sub> from FAPbI<sub>3</sub>. Illumination accelerates outgassing rates. Liberated organic gasses can contaminate line-of-sight surfaces, altering the optical properties of the vehicle and payload surfaces which can be detrimental to spacecraft performance [115]. Encapsulation of a device has been shown to slow outgassing [70] and use of a space qualified encapsulant has been shown to hold liberated compounds in proximity to the film to facilitate downstream healing [4]. Extended exposure to and operation in vacuum pressures has known impacts on perovskite solar cell material composition and electrical performance, impacting the overall lifetime of these cells in the space environment [14], [116], [117]. Exposure to vacuum decreases the operational lifetime of perovskite-based photovoltaics via outgassing and defect formation. Vacuum exposure also accelerates decomposition, phase segregation, and transitions at the grain boundaries. The grain boundary defects further accelerate ion migration across the device, another deleterious effect [116]. Ultimately, the stability of a perovskite absorber in vacuum depends on the device's chemical composition, configuration, processing method, and encapsulation.

**Table 3.** Atmospheric pressure at the surface of the planet in atmospheres (atm). The surfaces of Jupiter, Saturn, Uranus, and Neptune are deep in the atmosphere and the location and pressures are unknown.

Adapted from ref [41]

	Mercury	Venus	Earth	Lunar	Mars	Jupiter	Saturn	Uranus	Neptune	Pluto
Surface Pressure (atm)	0	91	1	0	0.1	unknown			0.00001	

#### 4.1. Summary

In this section, we summarize the vacuum pressures located at the varying space environments of interest. Extreme vacuum is a major risk to unprotected perovskites through outgassing and defect formation, in addition to accelerating material processes that decrease the lifetime and performance of the cell. Pressures in space will be orders of magnitude lower than pressures found on planetary/lunar surfaces. Stability in the vacuum environment should be a major target for optimization during the fabrication process as a relatively easy environmental condition to simulate.

### 5. Atomic Oxygen

Atomic (monatomic) oxygen is a highly reactive form of oxygen that can significantly degrade the performance of solar cells by reacting with or eroding materials. Atomic oxygen (AO) reacts with polymers and carbon containing materials typically creating CO and CO<sub>2</sub> as shown in **Figure 4A**. Organic materials are found in many high-performance perovskite-based photovoltaics as transport layers or barrier layers, but these materials should be avoided if possible, and they should never be used on an exposed surface. Despite enhancing photovoltaic power conversion efficiency, these volatile materials will introduce vulnerabilities that impact device durability. Metals and inorganic materials undergo surface oxidation which may lead to cracking or spalling which also negatively impact device performance over time [118], [119]. Unintended chemical reactions and/or physical erosion both disrupt the cell's electrical properties

reducing cell performance. There exist techniques to mitigate the negative impact of AO on materials including protective coatings, modified surface chemistry, and the use of getters. Careful materials selection is the most effective means of achieving a high efficiency perovskite-based photovoltaic that are robust performers in AO rich environments. **Figure 4B** summarizes all known environments (low Earth orbit, Mars, and Jovian moons) with atomic oxygen and reports the density of atomic oxygen as a function of distance [119], [120], [121]. Atomic oxygen is not a significant concern in GEO or lunar environments.

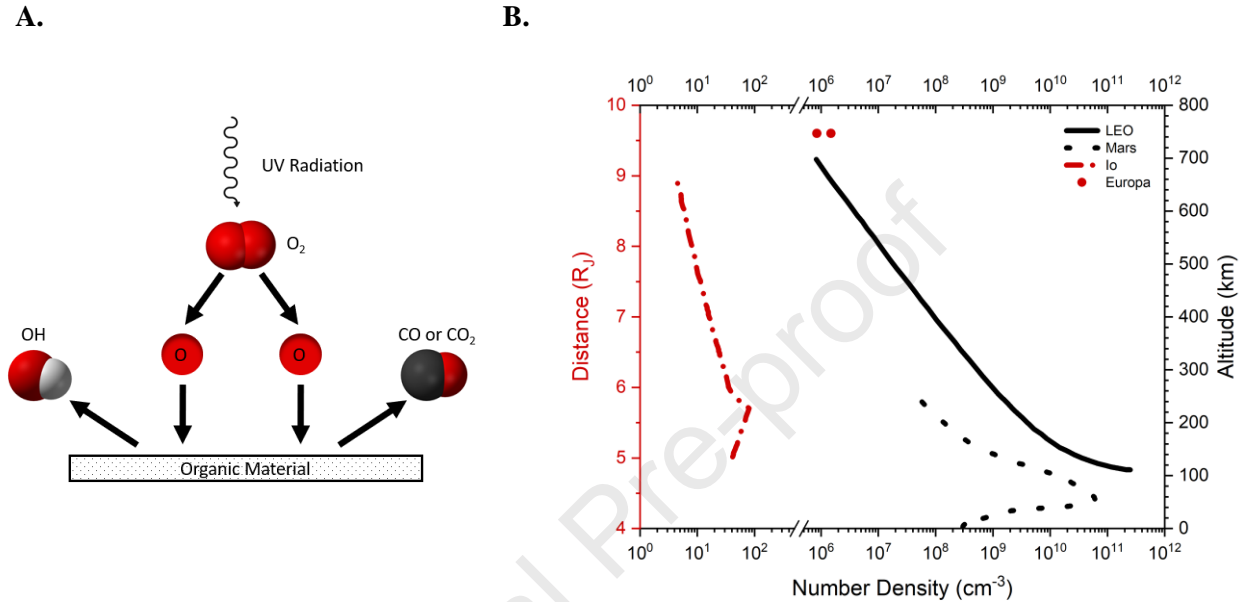


**Figure 4.** **A.** Basic atomic oxygen interaction with organic surfaces **B.** Density of atomic oxygen as a function of altitude from Earth (LEO) [118] and Mars surfaces [119] (black axis), and radial distance from Jupiter ( $1 R_J = 69,911$  km) for Jovian moons Io [120] and Europa [121] (red axis).

### 5.1. Low Earth Orbit (LEO)

Atomic oxygen (AO) is a highly reactive form of oxygen formed due to residual atmosphere in the Earth's thermosphere. AO is formed by photodissociation of diatomic oxygen when it is exposed to the Sun's ultraviolet radiation ( $\lambda < 243$  nm) in an environment where the atmospheric density is too low for competitive recombination processes to form diatomic oxygen, ozone, or nitrogen oxides.

Hydrocarbon based polymers and graphite are easily oxidized upon the impact of  $\sim 4.5$  eV atomic oxygen as spacecraft ram into the residual atmosphere of LEO [118]. AO is the most abundant species found within the LEO altitudes of 180-650 km and interacts with many materials flying in LEO. AO particle energies vary with altitude and typically range from 4-6 eV, providing sufficient energy to break chemical bonds and readily interact with incident materials. AO increases the diffuse reflectance of polymers due to surface texturing, breaks down and degrades organics and polymer chains, and oxidizes most metals. The AO erosion yields for various materials have been tabulated in reference [118]. The degree of surface degradation is directly proportional to the AO fluence which depends upon the spacecraft altitude, orbital inclination, mission duration, and solar activity [118], [122]. The solar cycle causes variation of the total level of atomic oxygen per year in LEO. In **Figure 5**, we show the variation at 400 km circular orbit,  $28.5^\circ$  inclination over two solar cycles.

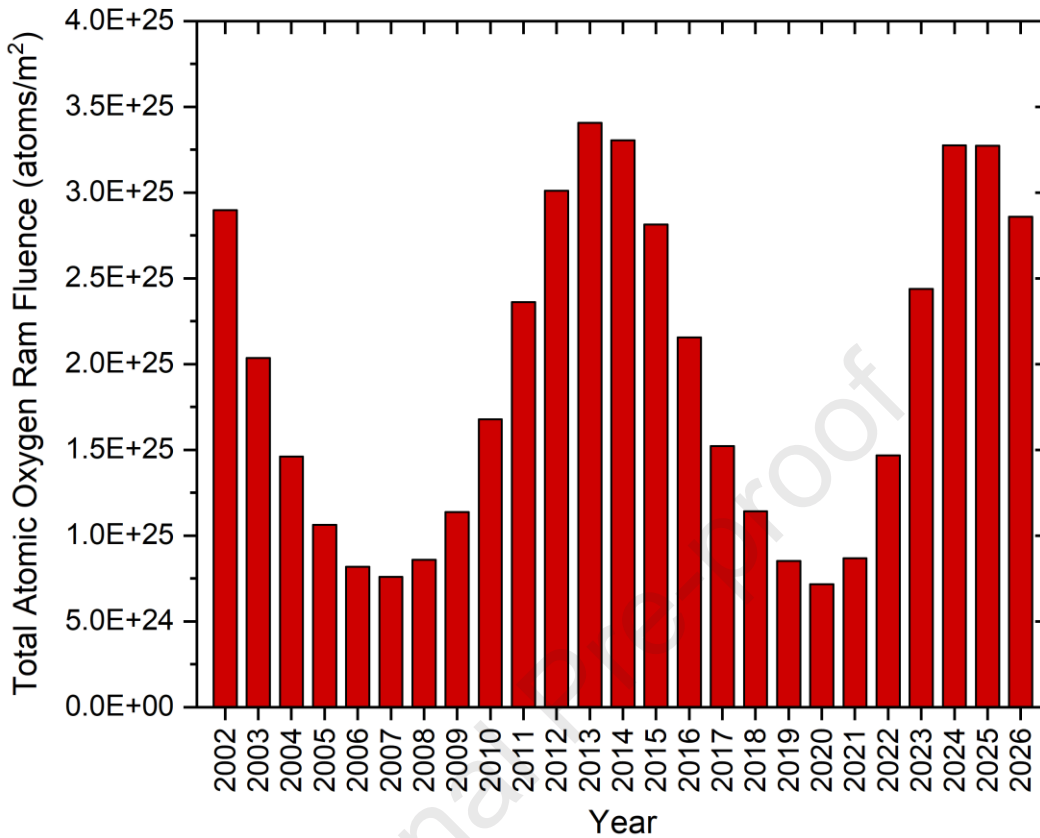


**Figure 5.** Solar cycle caused variation in total level of atomic oxygen per year in LEO at 400 km circular orbit, 28.5-degree inclination. (From Sharon K.R Miller, NASA Glenn Research Center, using MSIS-86 model)

In most cases, devices and materials can be protected from AO flux via encapsulation. These coatings often consist of metal oxide or metal thin films that are AO durable and prevent AO from reaching the underlying material. PV are often encapsulated with cover glass assemblies using a combination of adhesive/encapsulant, edge sealant and a cover glass. A protective coating of 1300 Å of sputtered SiO<sub>x</sub> (1.9 < x < 2) was applied to the International Space Station solar arrays' Kapton H blankets to significantly reduce the rate of oxidation of the underlying polymer [118]. The durability of a protective coating depends on the density and size of defects (pin hole and scratch) in the protective coating; increased defect densities permit AO attacks via undercutting oxidation at the defect sites. The best protection against AO is achieved by using smooth surface-level coatings with low defect density applied to just the space-exposed surface, resulting in less trapping of AO preserving the protected material [118]. The aforementioned protection mechanisms are suitable for perovskite-based photovoltaics deployed in atomic oxygen rich areas in any region of space.

## 5.2. Mars

Atomic oxygen, O, supersedes CO<sub>2</sub> as the prominent species above 200 km and up to the lower exosphere of Mars [123]. This indicates that protections against AO will need to be implemented to ensure that performance of perovskite solar cells doesn't rapidly degrade in the Martian atmosphere. The density of atomic oxygen as a function of altitude (km) from the Martian surface (in Mars low orbit, MLO) is depicted in Figure 4 as the black dashed line.

### 5.3. Interplanetary Space

Atomic oxygen production near Jupiter is primarily attributed to its moons Io and Europa. Io's atmosphere is largely made up of atomic oxygen and sulfur; as these particles undergo atmospheric sputtering and exit Io's exosphere, they can form neutral clouds around Jupiter [120]. Atomic oxygen forms a dense cloud (maximum number density of 80 cm<sup>-3</sup>) around the moon and a more diffuse cloud in the moon's orbit [120]. Europa's atmosphere has been found to emit atomic oxygen [121], [124], [125], [126]. The density of atomic oxygen as a function of radial distance from Jupiter (1 R<sub>J</sub>= 69,911 km) for Jovian moons Io [120] and Europa [121] is depicted in Figure 4 in red. Protections against AO will need to be implemented to ensure that perovskite-based photovoltaic performance is robust.

### 5.4. Summary:

In this section, we summarize the hazard that atomic oxygen poses to perovskites and highlight the specific environments in which it is present. AO is particularly damaging to many materials found in perovskite-based solar cells. Oxidation of metals, degradation of organics and polymers, and surface texturing of polymers by AO will greatly decrease the performance of lifetime of perovskites. Coatings to protect from AO have been investigated extensively due to its prevalence in the LEO environment. Encapsulation to protect from AO is strongly recommended for any perovskites operating in LEO, on the Martian surface, or at Jupiter and its moons Io and Europa.

## 6. Space Weather and Mechanical Stressors

Space weather broadly refers to changing conditions throughout the solar system, like varying solar wind, and meteoroid streams which affect planetary surfaces and volatile cycles. Solar flares and coronal mass ejections are naturally occurring events that result in stressors that can damage photovoltaics. The result of geomagnetic storms induced by coronal mass ejection include high energy particles and radiations. These effects are discussed briefly below, additional information on the impact of high energy radiation on perovskite-based photovoltaics is included in Section 3.

Dust storms that arise from changing conditions on a planetary body are another natural occurring phenomenon that impacts the operation of solar cells via erosion facilitated by abrasive regolith. Mechanical strength of photovoltaics for space applications is a frequently overlooked necessity. Cells manufactured on Earth and launched to their destination must endure vibrations from launch, flight, and landing. Further, as cells are deployed and stowed, they must endure bending without cracking. Micrometeorite and space debris impacts can also cause mechanical damage to photovoltaics once deployed in space. Cells must also endure erosion if they are employed in an environment that contains loose regolith or dust. AIAA S-111 has prescribed tests for mechanical strength of solar cells. The bend test calls for cells with an area of 20 cm<sup>2</sup> to be bent around a cylinder of 1500 mm radius under uniform pressure for no less than 10 seconds. A visual inspection at 10x magnification is then performed, any cell discrepancies including visual anomalies, cell cracks, chips, discoloration, and surface contamination shall be mapped. There is also a breaking load

determination where a cell is to be loaded and the flexural strength is computed in Pascals using equation 3, where P is the applied load in Newtons, L is the outer support span of the test fixture in meters, w is the width of the solar cell in meters, and t is the thickness of the solar cell in meters [69].

$$\sigma_f = \frac{3PL}{4wt^2} \quad \text{Equation 3}$$

The fracture of perovskite-based photovoltaics results in a loss of ohmic contact and creates an accelerated pathway for the diffusion of volatile organic compounds via outgassing. Ancillary layers significantly influence the mechanical stability of a perovskite-based photovoltaics and have been observed to be the primary source of mechanical failure [127]. Perovskite absorber layers have high coefficients of thermal expansion, six times greater than that of soda-lime glass, which provides an inherent stress sufficient to induce fracture [128]. This stress is increased by bending stresses or thermal cycling [5], [127]. One known mechanical weak point for perovskite devices is in the indium tin oxide (ITO) layer, which is brittle and upon flexion cracks propagate along the crystal grain boundaries. The organic charge transport layers within a device are a primary source of mechanical failure [5], [127]. It is recommended that during fabrication, conditions are controlled such that the resulting perovskite grain size is maximized as this results in greater mechanical stability. Further grain boundary engineering, via crosslinking crystalline domains, can further increase the fracture resistance of these materials by modestly improving the cohesion energy [127]. Altogether, precursor chemistry, stoichiometry, deposition technique, device design, and processing conditions are all factors in the resulting photovoltaic devices' mechanical stability.

### 6.1. Low Earth Orbit (LEO)

Space weather conditions can impact spacecraft in low earth orbit. In February 2022, 38 of the 49 SpaceX Starlink constellation satellites were lost due to the impacts of a geomagnetic storm that reached a 'minor' G1 intensity [129]. Every 11 years, the magnetic field of the Sun flips and the north and south poles interchange. During this periodic solar cycle, the activity on the Sun's surface changes; sunspots are initially absent, then increase over time, and finally decrease. The visual difference of the Sun's surface during maximum and minimum can be observed in Figure 6. As a result, there is an increase in radiation flux and magnetic field from the Sun through coronal mass ejections (CMEs) and solar energetic particles (SEPs). The ejected magnetic field links to Earth's geomagnetic field and transfers energy into Earth's magnetosphere. Some of this transferred energy is dissipated into the Earth's upper atmosphere. Resulting interactions lead to an increase in thermospheric density and the atmospheric drag acting on LEO satellites [129]. Geomagnetic storms have been classified by National Oceanic and Atmospheric Administration (NOAA) as summarized in reference [130]. These storms are infrequent but damaging to spacecrafts.

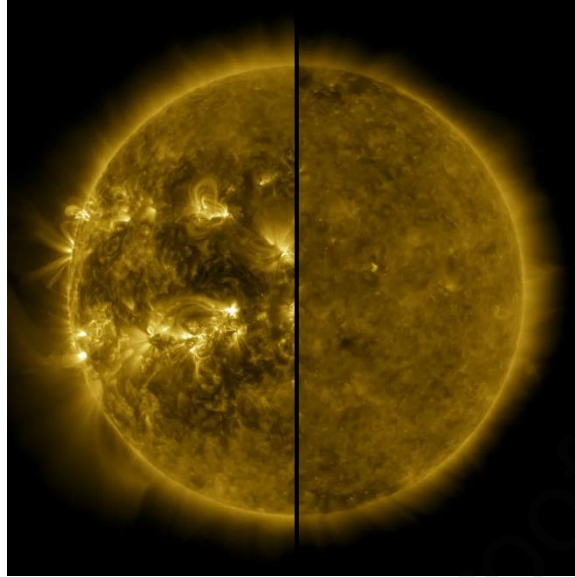


**Figure 6.** The difference in the surface of the Sun during solar maximum (left, captured April 2014) and solar minimum (right, captured December 2019). Credits: NASA/SDO [131].

Geomagnetic storms can cause extensive surface charging of satellites. Surface charging on a space craft can significantly impact perovskite-based photovoltaics via increasing the rate and magnitude of arcing on arrays. Arcing occurs when negative surfaces experience electrostatic discharges (ESD or arcs) either from surface to surface or directly into plasma once a critical threshold is exceeded. There are two types of plasma-related arcs that can occur in space. The first, a primary or trigger arc, is a transient event that discharges some spacecraft capacitance, generally on the order of microseconds. The second, a sustained arc, is precipitated by trigger arcs and are enabled by the solar array can occur between two solar array strings and may be powered by the array's current generating capacity [93]. Sustained arcs can cause substantial damage or destruction to photovoltaic arrays [132].

## 6.2. Geosynchronous Equatorial Orbit (GEO)

The Earth's magnetosphere traps high energy radiation particles, which form two distinct toroidal shaped belts of radiation known as the Van Allen Belts, as shown in **Figure 7**. Electrons have a two-zone structure, while megaelectron volt (MeV) ions are confined to the inner zone because of their larger gyroradii [133]. The highly stable inner radiation belt is located about 6000-12,000 km (1-2  $R_E$ ) above Earth's surface and is composed of relativistic and ultra-relativistic electrons with energies up to 10 MeV and protons with energies up to 700 MeV [134]. The density of the proton flux with energy  $>1$  MeV in the inner radiation belt is  $10^6$ - $10^7$   $\text{cm}^{-2}\text{s}^{-1}$  [135]. The inner zone proton belt is produced by a combination of cosmic ray albedo neutron decay (CRAND, where  $n \rightarrow H^+ + e^-$ ) and solar energetic protons associated with flares and coronal mass ejections. Solar energetic protons are the primary source at  $< 50$  MeV. The primary threat environment of the inner belt is 10's to 100's MeV protons. The two belts are separated by a slot region, an area with substantially smaller fluxes of particles. The outer radiation belt is located between 25,000-45,000 km (4-7 Earth radii,  $R_E$ ) above Earth's surface. It is composed of high-energy particles that originate from the sun. The outer radiation belt consists mostly of electrons whose energy is below 10 MeV. The density of the electron flux with energy  $>0.5$  MeV in the outer belt is up to  $10^9$   $\text{cm}^{-2}\text{s}^{-1}$  [135]. The outer radiation belt is

variable, sensitive to changes in the solar wind and geomagnetic activity. The electron concentration in the outer belt may vary as much as a factor of 1000. The primary threat of the outer belt is the 10's keV to 10's MeV electrons. If energetic electrons with sufficient flux charge materials faster than the charge can dissipate that accumulated charge density generates electric fields in excess of the breakdown strength resulting in electrostatic discharge. The system impact is material damage. The high energy electrons, protons, and ions in the outer belt result in high radiation exposures for perovskite-based photovoltaics powering satellites deployed in GEO.

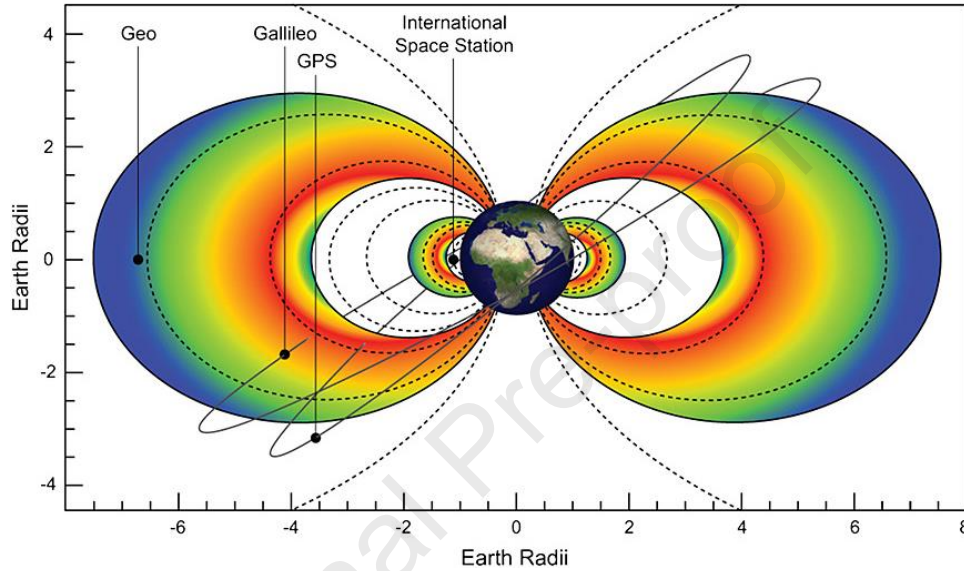


**Figure 7.** Different satellite orbits in relation to the Earth and the Earth's electron radiation belts. Most telecommunication satellites are in GEO, global navigation satellite system (GNSS) satellites such as Galileo and GPS are in medium Earth orbit (MEO), the international space station is in LEO. The slot region lies between the inner and outer radiation belts. The axes give distance from Earth in multiples of the Earth radius ( $1 R_E = 6378$  km). Reproduced with permission from [136]

### 6.3. Lunar

There is seismic activity on the Moon which could impact the structural components of perovskite-based solar arrays. Moonquakes are split into five categories: artificial impacts, meteoroid impacts, shallow quakes, deep quakes, and thermal quakes [137]. Artificial impacts result from spacecraft hitting the surface. Micrometeoroids are constantly striking the Moon's surface causing localized seismic activity. It is estimated that about  $10^6$  kg of material strike each year [138], with masses ranging from 100 g to 100 kg and  $2 \mu\text{m}$  to 2.5 m, respectively [139], [140]. Modeling predicts an average micrometeoroid flux of  $1.19 \times 10^{16}$  g/cm<sup>2</sup>·s across different regions of the Moon, with an average velocity ranging from 10- 72 km/s [138], [141]. Shallow moonquakes occur at a depth less than 200 km and are high frequency events; they are the most powerful recorded seismic events on the Moon with magnitudes ranging from 3.6 and 5.8 on the Richter scale [142]. Deep moonquakes occur between 700-1200 km and are tied to specific source regions; they are a common type of seismic activity and tend to be low magnitude. Thermal moonquakes correlate with temperature variations in the day-night cycle [143].

### 6.3.1. Lunar Dust

The charging processes on the Moon control the behavior of lunar dust, the smallest subset of lunar regolith. Lunar dust is classified as regolith with a particle size of 20  $\mu\text{m}$  and smaller. Particles are highly sharp because there are no natural erosion processes to erode and smooth the edges like those on Mars and Earth [101], [144]. The ionizing radiation environment can electrostatically loft lunar dust which facilitates dust deposition onto nearby surfaces [145], [146]. During the lunar day, the Moon is exposed to UV (UVC/UVB) light with an irradiance of 26.8  $\text{W}/\text{m}^2$  [147]. UV irradiation contributes to photoexcitation of lunar regolith [148], increasing scattering and lofting activity. Apollo astronauts observed these particles levitating above the surface and a “horizon glow” along the terminator as sunlight interacted with the lofted dust [101]. They also noted that dust was incredibly difficult to remove and proved to be a hinderance to ground operations [149]. This dust readily clings to surfaces and will coat the active surface of solar arrays, lowering power output due to reduced light absorption [150].

Dust can also be deposited on the perovskite-based solar arrays due to anthropogenic mechanisms through means like extravehicular activity (EVA), rover movement, or nearby vehicle landings [148]. Lunar landings can be particularly damaging due to plume surface interactions (PSI) where dust is ballistically accelerated away from a landing spacecraft [151], [152]. This can be highly damaging to arrays and other infrastructure. Lunar dust can also mechanically damage the surface through superficial scratching if it is removed improperly. Additionally, lunar dust is an insulator that will build up heat as it absorbs light due to its high solar absorbance [153], [154], creating problems for solar cells as the power conversion efficiency decreases as the temperature increases [155]. All these factors indicate that dust mitigation will be a critical aspect for arrays being implemented on the Moon and must be considered when developing surface manufacturing capabilities.

## 6.4. Mars

### 6.4.1. Mars Dust

The Martian atmosphere typically contains suspended dust. The levels of suspended dust in the atmosphere increases when global or local dust storms introduce dust into the atmosphere, decreases in mild weather conditions, and rarely approaches zero. Local dust storms can last a few days, regional storms can cover a large area, and global storms spread from the southern hemisphere during the southern hemisphere summer and can last for several months [24]. Dust storms have wind speeds up to 32  $\text{m}/\text{s}$  [156] and dust devils can reach heights of 10  $\text{km}$  [157]. Thus, all sunlight reaching Mars is filtered and scattered. The view of a dust storm from space is shown in **Figure 8**. Dust occultation will be an impactful variable to perovskite solar cell power output on Mars. Data from the Spirit and Opportunity rovers demonstrate the seasonal and irregular changes in  $\tau$  (optical depth) over many years [158]. Dust storms significantly affect power output, with drops of up to 85% for several months at a time [57]. Thus, the low power conversion efficiency of single-junction perovskites relative to triple-junction gallium arsenide (GaAs) cells, which were used on Spirit and Opportunity, may result in longer battery charging times and less available energy for a given mission or could necessitate the need for larger arrays. However, perovskite’s tunable bandgaps, 1.2 up to 3.1  $\text{eV}$ , are attractive options for top cells in tandem photovoltaics. Perovskite top cells would pair well with, perovskite, crystalline silicon (c-Si), or copper indium gallium selenide (CIGS) bottom cells [159], [160], [161]. Resulting light weight thin-film perovskite photovoltaic modules achieve competitive specific powers ( $\text{Watt}/\text{kg}$ ) when compared to III-V devices. As space resilient perovskite-tandem devices are developed, this performance gap should close.

Ground-based highly accelerated lifetime testing has shown that exposure to Mars dust storm conditions results in irreversible damage that manifests as  $V_{OC}$  losses and a reduction in minority carrier lifetimes [162]. These permanent performance losses are the result of high velocity dust impingement. Fortunately, the angle that solar cells are oriented to the ground impacts their dust accumulation, with 45-60° recommended to be the most robust orientations. Additionally, the wind that accompanies dust storms can cause flexure in solar arrays, so one may favor more rigid substrate materials [24]. Mars' increased distance from the Sun compared to the Earth results in a decreased solar power density. Viking Lander 1 reported a peak hourly global insolation (i.e., amount of solar radiation) of only 508 Whr/m<sup>2</sup>, roughly half that of Earth [163]. Design considerations for perovskite devices for operation in Mars should include a dust mitigation or management system and arrays must be sized appropriately to accommodate reduced incident light from global insolation and dust occultation.

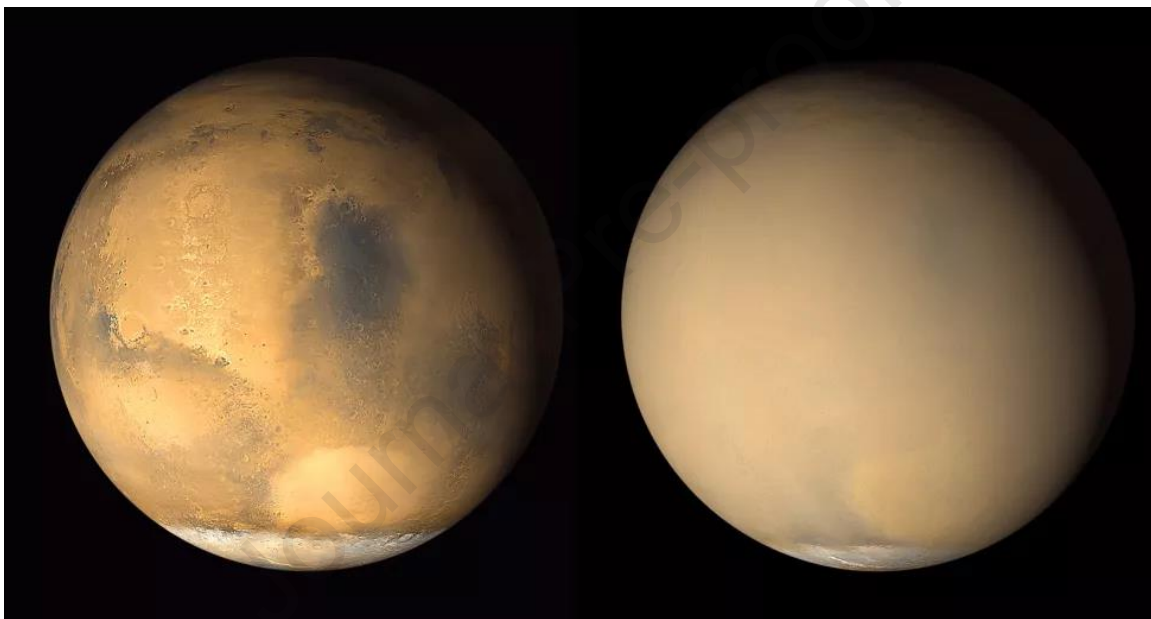


**Figure 8.** Haze engulfing Mars during a global dust storm. These two images were taken about a month apart in 2001. Photo from NASA's Mars Color Imager (MARCI) onboard Mars Reconnaissance Orbiter (MRO).

The presence of dust also dominates the electrostatic environment of Mars. Dust particle distribution has been sorted into three-components: atmospheric dust suspended for long periods of time with diameters 2-4  $\mu\text{m}$ , settled dust raised into the atmosphere by wind and dust devils (diameter  $\leq 10 \mu\text{m}$ ), and saltating particles with diameters greater than 80  $\mu\text{m}$  [164]. Dust levitated by storms and dust devils becomes electrostatically charged due to the multiple grain collisions in the dust-laden atmosphere [157]. Incident UV radiation on the Mars surface may electrostatically charge the stationary surface dust particles. Despite the total integrated UV flux over 200-400 nm being similar to Earth's, there is a greater contribution from shorter wavelengths to this flux on Mars [165]. Contact charging can also occur as a result of collisions between wind-blown dust particles and stationary surface particular matter [157]. Experiments have demonstrated that vertical motion of dust in a Mars simulated low-pressure CO<sub>2</sub> atmosphere can produce electric fields capable of creating electrical discharges which can be detected visually (glow) and

electronically [166], [167], [168]. Electrostatically charged dust adheres to surfaces, including the surfaces of solar cells thereby reducing their electrical output. Current solutions to manage dust occlusion for solar cells include careful selection of array angle [162] (recommended between 45-60°) and the inclusion of an electrodynamic dust shield which generates a traveling wave that acts as a contactless conveyor to accelerate charged dust particles [157], [169].

### **6.5. Interplanetary Space**

In our solar system, the gas giants (Jupiter and Saturn) and ice giants (Uranus and Neptune) lack surfaces for spacecraft to land. Their high pressures and extreme temperatures would crush and melt or vaporize any spacecraft that attempted to fly into the planet. Once we surmount the challenge of getting a spacecraft to survive near these planets, any perovskite-based photovoltaics must exhibit great radiation tolerance. The radiation doses are dependent on orbit, as discussed in Section 3. The photovoltaics must also have great mechanical strength to endure high winds. Jupiter has cyclones and distinctive belts with east to west winds reaching up to 575 km/hr [170]. Saturn's winds can reach up to 1800 km/hr. Uranus has windspeeds of up to 900 km/hr. Neptune's 2000 km/hr wind gusts make it our solar system's windiest planet [171].

### **6.6. Summary:**

In this section, we summarized the variety of natural phenomena and their resulting hazards in specific environments, ranging from lunar dust to micrometeoroids to windstorms on the gas and ice giants. The wide range of concerns covered in this section emphasizes the importance of understanding the risks of and designing perovskite-based solar array systems for a given mission environment. Dust found on the surface of the Moon and Mars can lower the power generated by the array through occlusion and cause mechanical damage to the cells themselves. High winds found on the outer planets and Mars and seismic activity on the Moon will all require both robust cell and array level systems. Micrometeoroids and geomagnetic storms can plague arrays operating both on and off planetary bodies. While it is not necessarily in the scope of perovskite solar cell research to address every potential environmental stressor, addressing the mechanical risks of a given space environment is an important factor in array design and mission proposal.

## **7. Conclusions**

We have thoroughly reviewed the environmental conditions of various regions in space that are impactful to the operation of perovskite solar cells. Perovskite-based photovoltaics are most promising for large area high voltage arrays and outer planetary satellite missions in LILT conditions. Mission profiles that include rapid thermal cycling will pose challenges for long duration operation. Careful attention must be paid to the selection of materials that discourage ion migration and are robust in the presence of atomic oxygen. Outgassing can be circumvented with careful materials design, selection, and encapsulation. Despite promising initial results, radiation environments still pose challenges to perovskite-based photovoltaic operation and thus require mission specific ground-based testing to validate durability in the applicable space theatre. Similarly, arcing and charging can be alleviated with material selection and diligent mission-specific coupon design and testing. Any photovoltaic system designed for deployment on the lunar or Mars surfaces will require dust mitigation. Dust mitigation can include active dust removal, or passive solutions such as encapsulation or array assembly at angles that impede dust adherence. Mechanical stressors are also unique to the mission; however, photovoltaic systems can be packaged to endure mechanical threats. Preliminary investigations of the greater perovskite space research community indicate that these materials can be designed and packaged to survive the space environment to which they will be deployed.

The design of photovoltaics for operation in space is mission specific. As such, the mission's duration, location, scientific goals, and operational requirements should be considered in the selection, design, and preparation of solar cells and array systems. All results thus far are very encouraging for the feasibility of perovskite-based photovoltaics for operation in space. More deeply understanding the contribution of each environmental factor on the perovskite-based photovoltaic devices will be critical. Combined environmental interactions can be more detrimental than the sum of their parts and must be investigated and considered, as well. We strongly recommend ground-based testing whenever possible, especially for the introduction of a novel photovoltaic material such as perovskites in a mission profile for which there is not heritage data. Progress in the basic science of perovskite-based photovoltaics in space theatres will be translatable to increasing the power conversion efficiency and stability of terrestrial cells.

## 8. Acknowledgements

The authors are grateful to Dr. Geoffrey Landis and Dr. Sharon Miller for insightful conversations on interplanetary space and atomic oxygen, respectively. The authors acknowledge NASA graphical artist Rodney Geschke for generating the graphic in Figure 1. The authors are grateful to the NASA Space Technology Mission Directorate for supporting this work through the following programs: The 2018 NASA Center Innovation Fund, and the 2019 Early Career Initiative. This work was authored in part by the National Renewable Energy Laboratory, operated by Alliance for Sustainable Energy, LLC, for the U.S. Department of Energy (DOE) under Contract No. DE-AC36-08GO28308. The NREL authors were supported through an interagency agreement with NASA. The views expressed in the article do not necessarily represent the views of the DOE or the U.S. Government.

## 9. References

- [1] A. R. Kirmani *et al.*, "Countdown to perovskite space launch: Guidelines to performing relevant radiation-hardness experiments," *Joule*, vol. 6, no. 5, pp. 1015–1031, May 2022, doi: 10.1016/j.joule.2022.03.004.
- [2] A. R. Kirmani *et al.*, "Unraveling radiation damage and healing mechanisms in halide perovskites using energy-tuned dual irradiation dosing," *Nat. Commun.*, vol. 15, no. 1, p. 696, Jan. 2024, doi: 10.1038/s41467-024-44876-1.
- [3] K. T. VanSant *et al.*, "Combined Stress Testing of Perovskite Solar Cells for Stable Operation in Space," *ACS Appl. Energy Mater.*, vol. 6, no. 20, pp. 10319–10326, Oct. 2023, doi: 10.1021/acsaem.2c03972.
- [4] W. Delmas *et al.*, "Evaluation of Hybrid Perovskite Prototypes After 10-Month Space Flight on the International Space Station," *Adv. Energy Mater.*, vol. 13, no. 19, p. 2203920, 2023, doi: 10.1002/aenm.202203920.
- [5] T. S. Krause, K. T. VanSant, A. Lininger, K. Crowley, T. J. Peshek, and L. McMillon-Brown, "Thermal Performance of Perovskite-Based Photovoltaics for Operation in Low Earth Orbit," *Sol. RRL*, vol. 7, no. 21, p. 2300468, 2023, doi: 10.1002/solr.202300468.
- [6] M. A. Green, A. Ho-Baillie, and H. J. Snaith, "The emergence of perovskite solar cells," *Nat. Photonics*, vol. 8, no. 7, Art. no. 7, Jul. 2014, doi: 10.1038/nphoton.2014.134.
- [7] "Pathways toward high-performance perovskite solar cells: review of recent advances in organo-metal halide perovskites for photovoltaic applications." Accessed: Oct. 21, 2019. [Online].

- Available: <https://www.spiedigitallibrary.org/journals/Journal-of-Photonics-for-Energy/volume-6/issue-2/022001/Pathways-toward-high-performance-perovskite-solar-cells--review-of/10.1117/1.JPE.6.022001.full>
- [8] H. Li and W. Zhang, "Perovskite Tandem Solar Cells: From Fundamentals to Commercial Deployment," *Chem. Rev.*, Aug. 2020, doi: 10.1021/acs.chemrev.9b00780.
- [9] H. Zhang, X. Ji, H. Yao, Q. Fan, B. Yu, and J. Li, "Review on efficiency improvement effort of perovskite solar cell," *Sol. Energy*, vol. 233, pp. 421–434, Feb. 2022, doi: 10.1016/j.solener.2022.01.060.
- [10] S. Sahare *et al.*, "Emerging Perovskite Solar Cell Technology: Remedial Actions for the Foremost Challenges," *Adv. Energy Mater.*, vol. 11, no. 42, p. 2101085, 2021, doi: 10.1002/aenm.202101085.
- [11] J. A. Christians, J. S. Manser, and P. V. Kamat, "Best Practices in Perovskite Solar Cell Efficiency Measurements. Avoiding the Error of Making Bad Cells Look Good," *J. Phys. Chem. Lett.*, vol. 6, no. 5, pp. 852–857, Mar. 2015, doi: 10.1021/acs.jpcclett.5b00289.
- [12] J. Ma and D. Guo, "A data review on certified perovskite solar cells efficiency and I-V metrics: Insights into materials selection and process scaling up," *Sol. Energy*, vol. 209, pp. 21–29, Oct. 2020, doi: 10.1016/j.solener.2020.08.090.
- [13] J. Yan, T. J. Savenije, L. Mazzarella, and O. Isabella, "Progress and challenges on scaling up of perovskite solar cell technology," *Sustain. Energy Fuels*, vol. 6, no. 2, pp. 243–266, 2022, doi: 10.1039/D1SE01045J.
- [14] D. Zhang, D. Li, Y. Hu, A. Mei, and H. Han, "Degradation pathways in perovskite solar cells and how to meet international standards," *Commun. Mater.*, vol. 3, no. 1, pp. 1–14, Aug. 2022, doi: 10.1038/s43246-022-00281-z.
- [15] R. Wang, M. Mujahid, Y. Duan, Z.-K. Wang, J. Xue, and Y. Yang, "A Review of Perovskites Solar Cell Stability," *Adv. Funct. Mater.*, vol. 29, no. 47, p. 1808843, 2019, doi: 10.1002/adfm.201808843.
- [16] J. Min, Y. Choi, D. Kim, and T. Park, "Beyond Imperfections: Exploring Defects for Breakthroughs in Perovskite Solar Cell Research," *Adv. Energy Mater.*, vol. 14, no. 6, p. 2302659, 2024, doi: 10.1002/aenm.202302659.
- [17] Q. Fatima, A. A. Haidry, H. Zhang, A. El Jery, and M. Aldrery, "A critical review on advancement and challenges in using TiO<sub>2</sub> as electron transport layer for perovskite solar cell," *Mater. Today Sustain.*, vol. 27, p. 100857, Sep. 2024, doi: 10.1016/j.mtsust.2024.100857.
- [18] V. Romano, A. Agresti, R. Verduci, and G. D'Angelo, "Advances in Perovskites for Photovoltaic Applications in Space," *ACS Energy Lett.*, vol. 7, no. 8, pp. 2490–2514, Aug. 2022, doi: 10.1021/acseenergylett.2c01099.
- [19] A. W. Y. Ho-Baillie *et al.*, "Deployment Opportunities for Space Photovoltaics and the Prospects for Perovskite Solar Cells," *Adv. Mater. Technol.*, vol. 7, no. 3, p. 2101059, 2022, doi: 10.1002/admt.202101059.
- [20] J. Yang, Q. Bao, L. Shen, and L. Ding, "Potential applications for perovskite solar cells in space," *Nano Energy*, vol. 76, p. 105019, Oct. 2020, doi: 10.1016/j.nanoen.2020.105019.
- [21] Y. Tu *et al.*, "Perovskite Solar Cells for Space Applications: Progress and Challenges," *Adv. Mater.*, vol. n/a, no. n/a, p. 2006545, doi: <https://doi.org/10.1002/adma.202006545>.
- [22] J. Plante and B. Lee, "Environmental Conditions for Space Flight Hardware: A Survey." Jan. 01, 2005. Accessed: May 23, 2024. [Online]. Available: <https://ntrs.nasa.gov/citations/20060013394>
- [23] L. McMillon-Brown, J. M. Luther, and T. J. Peshek, "What Would It Take to Manufacture Perovskite Solar Cells in Space?," *ACS Energy Lett.*, vol. 7, no. 3, pp. 1040–1042, Mar. 2022, doi: 10.1021/acseenergylett.2c00276.
- [24] G. Landis, T. Kerslake, P. Jenkins, and D. Scheiman, "Mars Solar Power," Dec. 2004, doi: 10.2514/6.2004-5555.

- [25] G. A. Landis and E. Haag, "Analysis of Solar Cell Efficiency for Venus Atmosphere and Surface Missions," in *11th International Energy Conversion Engineering Conference*, San Jose, CA: American Institute of Aeronautics and Astronautics, Jul. 2013. doi: 10.2514/6.2013-4028.
- [26] "Grandidier: Low-intensity high-temperature (LIHT)... - Google Scholar." Accessed: Mar. 14, 2025. [Online]. Available: [https://scholar.google.com/scholar\\_lookup?hl=en&volume=8&publication\\_year=2018&pages=1621-1626&journal=IEEE+J+Photovolt&issue=6&author=J+Grandidier&author=HA+Atwater&author=JA+Cutts&title=Low%E2%80%90Intensity+High%E2%80%90Temperature+%28LIHT%29+Solar+Cells+for+Venus+Atmosphere](https://scholar.google.com/scholar_lookup?hl=en&volume=8&publication_year=2018&pages=1621-1626&journal=IEEE+J+Photovolt&issue=6&author=J+Grandidier&author=HA+Atwater&author=JA+Cutts&title=Low%E2%80%90Intensity+High%E2%80%90Temperature+%28LIHT%29+Solar+Cells+for+Venus+Atmosphere)
- [27] J. Grandidier *et al.*, "Photovoltaic operation in the lower atmosphere and at the surface of Venus," *Prog. Photovolt. Res. Appl.*, vol. 28, no. 6, pp. 545–553, 2020, doi: 10.1002/pip.3214.
- [28] J. Berry *et al.*, "Hybrid Organic–Inorganic Perovskites (HOIPs): Opportunities and Challenges," *Adv. Mater.*, vol. 27, no. 35, pp. 5102–5112, 2015, doi: 10.1002/adma.201502294.
- [29] S. A. Kulkarni, T. Baikie, P. P. Boix, N. Yantara, N. Mathews, and S. Mhaisalkar, "Band-gap tuning of lead halide perovskites using a sequential deposition process," *J. Mater. Chem. A*, vol. 2, no. 24, pp. 9221–9225, 2014, doi: 10.1039/C4TA00435C.
- [30] F. Hao, C. C. Stoumpos, R. P. H. Chang, and M. G. Kanatzidis, "Anomalous Band Gap Behavior in Mixed Sn and Pb Perovskites Enables Broadening of Absorption Spectrum in Solar Cells," *J. Am. Chem. Soc.*, vol. 136, no. 22, pp. 8094–8099, Jun. 2014, doi: 10.1021/ja5033259.
- [31] Y. Ogomi *et al.*, "CH<sub>3</sub>NH<sub>3</sub>Sn<sub>x</sub>Pb(1–x)I<sub>3</sub> Perovskite Solar Cells Covering up to 1060 nm," *J. Phys. Chem. Lett.*, vol. 5, no. 6, pp. 1004–1011, Mar. 2014, doi: 10.1021/jz5002117.
- [32] E. Mosconi, P. Umari, and F. D. Angelis, "Electronic and optical properties of mixed Sn–Pb organohalide perovskites: a first principles investigation," *J. Mater. Chem. A*, vol. 3, no. 17, pp. 9208–9215, Apr. 2015, doi: 10.1039/C4TA06230B.
- [33] S. Kumar, M. M. R. Neidhe, F. Ahmed, and M. M. Hasan, "Enhancing Solar Cell Performance: The Impact of Microstructure in Nanostructured Perovskites," *Control Syst. Optim. Lett.*, vol. 3, no. 1, Art. no. 1, Jan. 2025, doi: 10.59247/csol.v3i1.136.
- [34] S. Wiegold *et al.*, "Precursor Concentration Affects Grain Size, Crystal Orientation, and Local Performance in Mixed-Ion Lead Perovskite Solar Cells," *ACS Appl. Energy Mater.*, vol. 1, no. 12, pp. 6801–6808, Dec. 2018, doi: 10.1021/acsaem.8b00913.
- [35] S. V. (ARC-P. E. & I. C. ] Weston, "Small Spacecraft Technology State of the Art 2024 report," 2025.
- [36] Y. P. Varshni, "Temperature dependence of the energy gap in semiconductors," *Physica*, vol. 34, no. 1, pp. 149–154, Jan. 1967, doi: 10.1016/0031-8914(67)90062-6.
- [37] L. Lin and N. M. Ravindra, "Temperature dependence of CIGS and perovskite solar cell performance: an overview," *SN Appl. Sci.*, vol. 2, no. 8, p. 1361, Jul. 2020, doi: 10.1007/s42452-020-3169-2.
- [38] "Potential of High-Stability Perovskite Solar Cells for Low-Intensity–Low-Temperature (LILT) Outer Planetary Space Missions | ACS Applied Energy Materials." Accessed: Dec. 09, 2020. [Online]. Available: [https://pubs.acs.org/doi/abs/10.1021/acsaem.8b01882?casa\\_token=7O65Jo0aBc0AAAAA:vhrYXPv0dC3RGgkSUMi4Y1FLCYwj5mK0jINn\\_HF4IAGZofy0\\_Ignb9rmCACybJ6OZ8uX6kDGqTCJdcbb](https://pubs.acs.org/doi/abs/10.1021/acsaem.8b01882?casa_token=7O65Jo0aBc0AAAAA:vhrYXPv0dC3RGgkSUMi4Y1FLCYwj5mK0jINn_HF4IAGZofy0_Ignb9rmCACybJ6OZ8uX6kDGqTCJdcbb)
- [39] Z. Xiao and Y. Yan, "Progress in Theoretical Study of Metal Halide Perovskite Solar Cell Materials," *Adv. Energy Mater.*, vol. 7, no. 22, p. 1701136, 2017, doi: 10.1002/aenm.201701136.
- [40] H. Zhang, X. Qiao, Y. Shen, and M. Wang, "Effect of temperature on the efficiency of organometallic perovskite solar cells," *J. Energy Chem.*, vol. 24, no. 6, pp. 729–735, Nov. 2015, doi: 10.1016/j.jechem.2015.10.007.

- [41] “Planetary Fact Sheet - U.S. Units.” Accessed: Nov. 12, 2024. [Online]. Available: [https://nssdc.gsfc.nasa.gov/planetary/factsheet/planet\\_table\\_british.html](https://nssdc.gsfc.nasa.gov/planetary/factsheet/planet_table_british.html)
- [42] M. C. Alonso García and J. L. Balenzategui, “Estimation of photovoltaic module yearly temperature and performance based on Nominal Operation Cell Temperature calculations,” *Renew. Energy*, vol. 29, no. 12, pp. 1997–2010, Oct. 2004, doi: 10.1016/j.renene.2004.03.010.
- [43] G. J. Thaikattil, S. Jansen, M. Deminico, M. Y. Sinaki, J. S. McNatt, and T. Peshek, “Thermal Analysis of Photovoltaic Investigation on the Lunar Surface (PILS),” in *AIAA Propulsion and Energy 2021 Forum*, American Institute of Aeronautics and Astronautics. doi: 10.2514/6.2021-3257.
- [44] T. Matsui *et al.*, “Compositional Engineering for Thermally Stable, Highly Efficient Perovskite Solar Cells Exceeding 20% Power Conversion Efficiency with 85 °C/85% 1000 h Stability,” *Adv. Mater.*, vol. 31, no. 10, p. 1806823, 2019, doi: 10.1002/adma.201806823.
- [45] Q. Meng *et al.*, “Effect of temperature on the performance of perovskite solar cells,” *J. Mater. Sci. Mater. Electron.*, vol. 32, no. 10, pp. 12784–12792, May 2021, doi: 10.1007/s10854-020-03029-y.
- [46] C. Quarti *et al.*, “Structural and optical properties of methylammonium lead iodide across the tetragonal to cubic phase transition: implications for perovskite solar cells,” *Energy Environ. Sci.*, vol. 9, no. 1, pp. 155–163, 2016, doi: 10.1039/C5EE02925B.
- [47] T. Baikie *et al.*, “Synthesis and crystal chemistry of the hybrid perovskite (CH<sub>3</sub>NH<sub>3</sub>)PbI<sub>3</sub> for solid-state sensitised solar cell applications,” *J. Mater. Chem. A*, vol. 1, no. 18, pp. 5628–5641, Apr. 2013, doi: 10.1039/C3TA10518K.
- [48] W. Geng, L. Zhang, Y.-N. Zhang, W.-M. Lau, and L.-M. Liu, “First-Principles Study of Lead Iodide Perovskite Tetragonal and Orthorhombic Phases for Photovoltaics,” *J. Phys. Chem. C*, vol. 118, no. 34, pp. 19565–19571, Aug. 2014, doi: 10.1021/jp504951h.
- [49] K. W. Tan *et al.*, “Thermally Induced Structural Evolution and Performance of Mesoporous Block Copolymer-Directed Alumina Perovskite Solar Cells,” *ACS Nano*, vol. 8, no. 5, pp. 4730–4739, May 2014, doi: 10.1021/nn500526t.
- [50] S. Kim *et al.*, “Relationship between ion migration and interfacial degradation of CH<sub>3</sub>NH<sub>3</sub>PbI<sub>3</sub> perovskite solar cells under thermal conditions,” *Sci. Rep.*, vol. 7, no. 1, p. 1200, Apr. 2017, doi: 10.1038/s41598-017-00866-6.
- [51] B. J. Anderson, C. G. Justus, and G. W. Batts, “Guidelines for the Selection of Near-Earth Thermal Environment Parameters for Spacecraft Design,” NASA/TM-2001-211221, Oct. 2001. Accessed: May 23, 2024. [Online]. Available: <https://ntrs.nasa.gov/citations/20020004360>
- [52] K. K. Degroh, B. A. Banks, and D. C. Smith, “Environmental Durability Issues for Solar Power Systems in Low Earth Orbit,” presented at the 1995 International Solar Energy Conference, Lahaina, HI, Nov. 1994. Accessed: May 23, 2024. [Online]. Available: <https://ntrs.nasa.gov/citations/19950009355>
- [53] J.-P. Williams, D. A. Paige, B. T. Greenhagen, and E. Sefton-Nash, “The global surface temperatures of the Moon as measured by the Diviner Lunar Radiometer Experiment,” *Icarus*, vol. 283, pp. 300–235, Feb. 2017, doi: doi.org/10.1016/j.icarus.2016.08.012.
- [54] J. Fincannon, “Characterization of Lunar Polar Illumination from a Power System Perspective,” in *46th AIAA Aerospace Sciences Meeting and Exhibit*, in Aerospace Sciences Meetings. , American Institute of Aeronautics and Astronautics, 2008. doi: 10.2514/6.2008-447.
- [55] A. Delgado-Bonal and F. J. Martín-Torres, “Solar cell temperature on Mars,” *Sol. Energy*, vol. 118, pp. 74–79, Aug. 2015, doi: 10.1016/j.solener.2015.04.035.
- [56] “Temperatures Across Our Solar System - NASA Science.” Accessed: May 08, 2024. [Online]. Available: <https://science.nasa.gov/solar-system/temperatures-across-our-solar-system/>
- [57] P. M. Stella and J. A. Herman, “The Mars surface environment and solar array performance,” in *2010 35th IEEE Photovoltaic Specialists Conference*, Jun. 2010, pp. 002631–002635. doi: 10.1109/PVSC.2010.5617185.

- [58] Planetary Science Program, "Solar Power Technologies for Future Planetary Science Missions," JPL, Strategic Missions and Advanced Concepts Office Solar System Exploration Directorate Jet Propulsion Laboratory for Planetary Science Division Science Mission Directorate NASA JPL D-101316, Dec. 2017. Accessed: Nov. 02, 2022. [Online]. Available: <https://solarsystem.nasa.gov/resources/548/solar-power-technologies-for-future-planetary-science-missions>
- [59] A. Boca, "Solar Cell Testing for the Jupiter Environment: Low Irradiance, Low Temperature and High Radiation," in *2019 IEEE 46th Photovoltaic Specialists Conference (PVSC)*, Chicago, IL, USA: IEEE, Jun. 2019, pp. 2787–2791. doi: 10.1109/PVSC40753.2019.8981342.
- [60] N. Strange, T. Spilker, D. Landau, T. Lam, D. Lyons, and J. Guzman, "Mission design for the titan saturn system mission concept," *Adv. Astronaut. Sci.*, vol. 135, no. 2, pp. 919–934, 2009.
- [61] A. Boca, R. Warwick, B. White, and R. Ewell, "A Data-Driven Evaluation of the Viability of Solar Arrays at Saturn," *IEEE J. Photovolt.*, vol. 7, no. 4, pp. 1159–1164, Jul. 2017, doi: 10.1109/JPHOTOV.2017.2698499.
- [62] C. R. Brown, G. E. Eperon, V. R. Whiteside, and I. R. Sellers, "Potential of High-Stability Perovskite Solar Cells for Low-Intensity–Low-Temperature (LILT) Outer Planetary Space Missions," *ACS Appl. Energy Mater.*, vol. 2, no. 1, pp. 814–821, Jan. 2019, doi: 10.1021/acsaem.8b01882.
- [63] R. T. Ginting, E.-S. Jung, M.-K. Jeon, W.-Y. Jin, M. Song, and J.-W. Kang, "Low-temperature operation of perovskite solar cells: With efficiency improvement and hysteresis-less," *Nano Energy*, vol. 27, pp. 569–576, Sep. 2016, doi: 10.1016/j.nanoen.2016.08.016.
- [64] A. Bocca, C. MacFarland, and R. Kowalczyk, "Solar Power for Deep-Space Applications: State of Art and Deployment," in *AIAA 2019-4236*, Indianapolis, IN, Aug. 2019. doi: <https://doi.org/10.2514/6.2019-4236>.
- [65] G. D. Badhwar, "The Radiation Environment in Low-Earth Orbit," *Radiat. Res.*, vol. 148, no. 5, pp. S3–S10, 1997, doi: 10.2307/3579710.
- [66] J. L. Le Mouël, F. Lopes, and V. Courtillot, "Characteristic Time Scales of Decadal to Centennial Changes in Global Surface Temperatures Over the Past 150 Years," *Earth Space Sci.*, vol. 7, no. 4, p. e2019EA000671, 2020, doi: 10.1029/2019EA000671.
- [67] P. Väisänen, I. Usoskin, and K. Mursula, "Long-Term and Solar Cycle Variation of Galactic Cosmic Rays: Evidence for Variable Heliospheric Turbulence," *J. Geophys. Res. Space Phys.*, vol. 124, no. 2, pp. 804–811, 2019, doi: 10.1029/2018JA026135.
- [68] G. Drolshagen, A. Hilgers, and H. Evans, "Space Environment Analysis: Experience and Trends," vol. 392, p. 15, Nov. 1996.
- [69] "AIAA S-111A-2014 - Qualification and Quality Requirements for Space Solar Cells." Accessed: Nov. 01, 2023. [Online]. Available: [https://webstore.ansi.org/standards/aiaa/aiaa111a2014?source=blog&\\_gl=1\\*18xwejd\\*\\_gcl\\_au\\*MjA2MjYONjlxNC4xNjk3NzM2NDk2](https://webstore.ansi.org/standards/aiaa/aiaa111a2014?source=blog&_gl=1*18xwejd*_gcl_au*MjA2MjYONjlxNC4xNjk3NzM2NDk2)
- [70] Y. Miyazawa *et al.*, "Tolerance of Perovskite Solar Cell to High-Energy Particle Irradiations in Space Environment," *iScience*, vol. 2, pp. 148–155, Apr. 2018, doi: 10.1016/j.isci.2018.03.020.
- [71] F. Lang *et al.*, "Proton Radiation Hardness of Perovskite Tandem Photovoltaics," *Joule*, vol. 4, no. 5, pp. 1054–1069, May 2020, doi: 10.1016/j.joule.2020.03.006.
- [72] B. K. Durant, H. Afshari, S. Singh, B. Rout, G. E. Eperon, and I. R. Sellers, "Tolerance of Perovskite Solar Cells to Targeted Proton Irradiation and Electronic Ionization Induced Healing," *ACS Energy Lett.*, vol. 6, no. 7, pp. 2362–2368, Jul. 2021, doi: 10.1021/acsenenergylett.1c00756.
- [73] F. Lang *et al.*, "Proton-Radiation Tolerant All-Perovskite Multijunction Solar Cells," *Adv. Energy Mater.*, vol. 11, no. 41, p. 2102246, 2021, doi: 10.1002/aenm.202102246.

- [74] B. K. Durant *et al.*, "Radiation stability of mixed tin–lead halide perovskites: Implications for space applications," *Sol. Energy Mater. Sol. Cells*, vol. 230, p. 111232, Sep. 2021, doi: 10.1016/j.solmat.2021.111232.
- [75] J. Huang *et al.*, "Effects of Electron and Proton Radiation on Perovskite Solar Cells for Space Solar Power Application," in *2017 IEEE 44th Photovoltaic Specialist Conference (PVSC)*, Jun. 2017, pp. 1248–1252. doi: 10.1109/PVSC.2017.8366410.
- [76] F. Lang *et al.*, "Radiation Hardness and Self-Healing of Perovskite Solar Cells," *Adv. Mater.*, vol. 28, no. 39, pp. 8726–8731, 2016, doi: <https://doi.org/10.1002/adma.201603326>.
- [77] V. V. Brus *et al.*, "Defect Dynamics in Proton Irradiated CH<sub>3</sub>NH<sub>3</sub>PbI<sub>3</sub> Perovskite Solar Cells," *Adv. Electron. Mater.*, vol. 3, no. 2, p. 1600438, 2017, doi: <https://doi.org/10.1002/aelm.201600438>.
- [78] J. Barbé *et al.*, "Radiation Hardness of Perovskite Solar Cells Based on Aluminum-Doped Zinc Oxide Electrode Under Proton Irradiation," *Sol. RRL*, vol. 3, no. 12, p. 1900219, 2019, doi: <https://doi.org/10.1002/solr.201900219>.
- [79] F. Lang *et al.*, "Efficient minority carrier detrapping mediating the radiation hardness of triple-cation perovskite solar cells under proton irradiation," *Energy Environ. Sci.*, vol. 12, no. 5, pp. 1634–1647, May 2019, doi: 10.1039/C9EE00077A.
- [80] O. Malinkiewicz, M. Imaizumi, S. B. Sapkota, T. Ohshima, and S. Öz, "Radiation effects on the performance of flexible perovskite solar cells for space applications," *Emergent Mater.*, vol. 3, no. 1, pp. 9–14, Feb. 2020, doi: 10.1007/s42247-020-00071-8.
- [81] G. M. Paternò *et al.*, "Perovskite solar cell resilience to fast neutrons," *Sustain. Energy Fuels*, vol. 3, no. 10, pp. 2561–2566, 2019, doi: 10.1039/C9SE00102F.
- [82] K. Yang *et al.*, "Radiation tolerance of perovskite solar cells under gamma ray," *Org. Electron.*, vol. 71, pp. 79–84, Aug. 2019, doi: 10.1016/j.orgel.2019.05.008.
- [83] A. G. Boldyreva *et al.*, "γ-Ray-Induced Degradation in the Triple-Cation Perovskite Solar Cells," *J. Phys. Chem. Lett.*, vol. 10, no. 4, pp. 813–818, Feb. 2019, doi: 10.1021/acs.jpcclett.8b03222.
- [84] A. G. Boldyreva *et al.*, "Unravelling the Material Composition Effects on the Gamma Ray Stability of Lead Halide Perovskite Solar Cells: MAPbI<sub>3</sub> Breaks the Records," *J. Phys. Chem. Lett.*, vol. 11, no. 7, pp. 2630–2636, Apr. 2020, doi: 10.1021/acs.jpcclett.0c00581.
- [85] B. Vayner, J. Galofaro, and D. Ferguson, "Interactions of High-Voltage Solar Arrays with Their Plasma Environment: Physical Processes," *J. Spacecr. Rockets*, vol. 41, no. 6, Dec. 2004.
- [86] B. V. Vayner, "Solar Array in Dense Plasma," American Institute of Aeronautics and Astronautics, Jan. 2014. doi: 10.2514/6.2014-1421.
- [87] B. Vayner and J. T. Galofaro, "Inception and Prevention of Sustained Discharges on Solar Arrays," *IEEE Trans. Plasma Sci.*, vol. 40, no. 2, pp. 388–393, Feb. 2012, doi: 10.1109/TPS.2011.2177480.
- [88] "NASA-HDBK-4002 | NASA Technical Standards System (NTSS)." Accessed: Nov. 14, 2017. [Online]. Available: <https://standards.nasa.gov/standard/nasa/nasa-hdbk-4002>
- [89] "NASA-HDBK-4006 | NASA Technical Standards System (NTSS)." Accessed: Nov. 14, 2017. [Online]. Available: <https://standards.nasa.gov/standard/nasa/nasa-hdbk-4006>
- [90] 14:00-17:00, "ISO 11221:2011," ISO. Accessed: Sep. 13, 2024. [Online]. Available: <https://www.iso.org/standard/50296.html>
- [91] D. C. Ferguson, B. V. Vayner, J. T. Galofaro, G. Hillard, J. Vaughn, and T. Schneider, "NASA GRC and MSFC Space Plasma Arc Testing Procedures," *IEEE Trans. Plasma Sci.*, vol. 34, no. 5, pp. 1948–1948, Oct. 2006, doi: 0.1109/TPS.2006.879093.
- [92] B. Vayner, J. Galofaro, and D. Ferguson, "Solar array in simulated LEO plasma environment," 2003, Accessed: Apr. 11, 2017. [Online]. Available: <https://ntrs.nasa.gov/search.jsp?R=20040027858>
- [93] D. C. Ferguson, B. V. Vayner, J. T. Galofaro, and G. B. Hillard, "Arcing in LEO: Does the Whole Array Discharge?," Jan. 01, 2005. Accessed: May 06, 2024. [Online]. Available: <https://ntrs.nasa.gov/citations/20050182910>

- [94] B. Reddell, J. Alred, L. Kramer, R. Mikatariyan, J. Minow, and S. Koontz, "Analysis of ISS plasma interaction," 2006, Accessed: Aug. 22, 2017. [Online]. Available: <https://arc.aiaa.org/doi/pdf/10.2514/6.2006-865>
- [95] J. D. Williams, C. C. Farnell, P. B. Shoemaker, J. A. Vaughn, and T. A. Schneider, "GROUND-BASED SIMULATION OF LOW EARTH ORBIT PLASMA CONDITIONS: PLASMA GENERATION AND CHARACTERIZATION".
- [96] P. C. Anderson, "Characteristics of spacecraft charging in low Earth orbit," *J. Geophys. Res. Space Phys.*, vol. 117, no. A7, p. A07308, Jul. 2012, doi: 10.1029/2011JA016875.
- [97] "SPENVIS - Space Environment, Effects, and Education System." Accessed: Jul. 23, 2024. [Online]. Available: <https://www.spennis.oma.be/>
- [98] M. Bodeau, "Current and Voltage Thresholds for Sustained Arcs in Power Systems," *IEEE Trans. Plasma Sci.*, vol. 40, no. 2, Feb. 2012, doi: 10.1109/TPS.2011.2176932.
- [99] T. J. Stubbs, J. S. Halekas, W. M. Farrell, and R. R. Vondrak, "Lunar Surface Charging: A Global Perspective Using Lunar Prospector Data," vol. 643, pp. 181–184, Jan. 2007.
- [100] E. Kallio, S. Dyadechkin, P. Wurz, and M. Khodachenko, "Space weathering on the Moon: Farside-nearside solar wind precipitation asymmetry," *Planet. Space Science*, vol. 166, pp. 9–22, Feb. 2019, doi: <https://doi.org/10.1016/j.pss.2018.07.013>.
- [101] G. H. Heiken, D. T. Vaniman, and B. M. French, *Lunar Sourcebook: A User's Guide to the Moon*. Cambridge University Press, 1991. [Online]. Available: [https://www.lpi.usra.edu/publications/books/lunar\\_sourcebook/pdf/LunarSourceBook.pdf](https://www.lpi.usra.edu/publications/books/lunar_sourcebook/pdf/LunarSourceBook.pdf)
- [102] M. N. Rao, D. H. Garrison, D. D. Bogard, and R. C. Reedy, "Determination of the flux and energy distribution of energetic solar protons in the past 2 Myr using lunar rock 68815," *Geochim. Cosmochim. Acta*, vol. 58, no. 19, pp. 4231–4245, 1994.
- [103] G. Reitz, T. Berger, and D. Matthiae, "Radiation exposure in the moon environment," *Planet. Space Sci.*, vol. 74, pp. 78–83, 2012, doi: 10.1016/j.pss.2012.07.014.
- [104] S. T. Crites, P. G. Lucey, and D. J. Lawrence, "Proton flux and radiation dose from galactic cosmic rays in the lunar regolith and implications for organic synthesis at the poles of the Moon and Mercury," *Icarus*, vol. 226, pp. 1192–1200, 2013, doi: 10.1016/j.icarus.2013.08.003.
- [105] C. Zeitlin *et al.*, "Overview of the Martian radiation environment experiment," *Adv. Space Res. Off. J. Comm. Space Res. COSPAR*, vol. 33, no. 12, pp. 2204–2210, 2004, doi: 10.1016/s0273-1177(03)00514-3.
- [106] T. C. Slaba, C. J. Mertens, and S. R. Blattnig, "Radiation Shielding Optimization on Mars." Apr. 01, 2013. Accessed: Jun. 06, 2024. [Online]. Available: <https://ntrs.nasa.gov/citations/20130012456>
- [107] K. Khurana and et al, "Ch. 24 The Configuration of Jupiter's Magnetosphere," in *Jupiter: The planet, satellites and magnetosphere*, 2004, pp. 593–616.
- [108] J. E. P. Connerney *et al.*, "Jupiter's magnetosphere and aurorae observed by the Juno spacecraft during its first polar orbits," *Science*, vol. 356, no. 6340, pp. 826–832, May 2017, doi: 10.1126/science.aam5928.
- [109] N. Krupp and et al., "Ch. 25 Dynamics of the Jovian Magnetosphere," in *Jupiter: The planet, satellites and magnetosphere*, 2004, pp. 617–638.
- [110] W. Atwell, "Radiation Environments for Deep-Space Missions and Exposure Estimates," in *AIAA SPACE 2007 Conference & Exposition*, Long Beach, California: American Institute of Aeronautics and Astronautics, Sep. 2007. doi: 10.2514/6.2007-6044.
- [111] "Trapped Particle Environments of the Outer Planets | IEEE Journals & Magazine | IEEE Xplore." Accessed: Nov. 22, 2024. [Online]. Available: <https://ieeexplore.ieee.org/abstract/document/8692760>

- [112] E. Grossman and I. Gouzman, "Space environment effects on polymers in low earth orbit," *Nucl. Instrum. Methods Phys. Res. Sect. B Beam Interact. Mater. At.*, vol. 208, pp. 48–57, Aug. 2003, doi: 10.1016/S0168-583X(03)00640-2.
- [113] E. J. Juarez-Perez, L. K. Ono, M. Maeda, Y. Jiang, Z. Hawash, and Y. Qi, "Photodecomposition and thermal decomposition in methylammonium halide lead perovskites and inferred design principles to increase photovoltaic device stability," *J. Mater. Chem. A*, vol. 6, no. 20, pp. 9604–9612, May 2018, doi: 10.1039/C8TA03501F.
- [114] E. J. Juarez-Perez, L. K. Ono, and Y. Qi, "Thermal degradation of formamidinium based lead halide perovskites into sym-triazine and hydrogen cyanide observed by coupled thermogravimetry-mass spectrometry analysis," *J. Mater. Chem. A*, vol. 7, no. 28, pp. 16912–16919, Jul. 2019, doi: 10.1039/C9TA06058H.
- [115] M. M. Finckenor and K. de Groh, "A researcher's guide to: space environmental effects," *Natl. Aeronaut. Space Adm. Int. Space Stn. Res. Guide Ser. NP-2015-03-015-ISC*, p. 15, 2017.
- [116] Y. Jiang *et al.*, "Mitigation of Vacuum and Illumination-Induced Degradation in Perovskite Solar Cells by Structure Engineering," *Joule*, vol. 4, no. 5, pp. 1087–1103, May 2020, doi: 10.1016/j.joule.2020.03.017.
- [117] L. J. Sutherland *et al.*, "Effect of out-gassing from polymeric encapsulant materials on the lifetime of perovskite solar cells," *Sol. Energy Mater. Sol. Cells*, vol. 246, p. 111887, Oct. 2022, doi: 10.1016/j.solmat.2022.111887.
- [118] B. A. Banks, K. K. deGroh, and S. K. Miller, "Low Earth Orbital Atomic Oxygen Interactions With Spacecraft Materials," E-14905, Nov. 2004. Accessed: Nov. 09, 2022. [Online]. Available: <https://ntrs.nasa.gov/citations/20040191331>
- [119] S. K. R. Miller and B. A. Banks, "Atomic Oxygen Environment and Effects Overview," Accessed: May 08, 2024. [Online]. Available: <https://ntrs.nasa.gov/citations/20210023367>
- [120] R. Koga *et al.*, "Spatial Distribution of Io's Neutral Oxygen Cloud Observed by Hisaki," *J. Geophys. Res. Space Phys.*, vol. 123, no. 5, pp. 3764–3776, 2018, doi: 10.1029/2018JA025328.
- [121] C. J. Hansen, D. E. Shemansky, and A. R. Hendrix, "Cassini UVIS observations of Europa's oxygen atmosphere and torus," *Icarus*, vol. 176, no. 2, pp. 305–315, Aug. 2005, doi: 10.1016/j.icarus.2005.02.007.
- [122] S. W. Samwel, "Low earth orbital atomic oxygen erosion effect on spacecraft materials," *Space Res J*, vol. 7, no. 1, pp. 1–13, 2014.
- [123] J. Qin, "Mars Upper Atmospheric Temperature and Atomic Oxygen Density Derived from the O i 130.4 nm Emission Observed by NASA's MAVEN Mission," *Astron. J.*, vol. 159, no. 5, p. 206, Apr. 2020, doi: 10.3847/1538-3881/ab7fae.
- [124] D. T. Hall, D. F. Strobel, P. D. Feldman, M. A. McGrath, and H. A. Weaver, "Detection of an oxygen atmosphere on Jupiter's moon Europa," *Nature*, vol. 373, no. 6516, pp. 677–679, Feb. 1995, doi: 10.1038/373677a0.
- [125] "Europa's far ultraviolet oxygen aurora from a comprehensive set of HST observations - Roth - 2016 - Journal of Geophysical Research: Space Physics - Wiley Online Library." Accessed: Nov. 04, 2024. [Online]. Available: <https://agupubs.onlinelibrary.wiley.com/doi/full/10.1002/2015JA022073>
- [126] K. de Kleer, Z. Milby, C. Schmidt, M. Camarca, and M. E. Brown, "The Optical Aurorae of Europa, Ganymede, and Callisto," *Planet. Sci. J.*, vol. 4, no. 2, p. 37, Feb. 2023, doi: 10.3847/PSJ/acb53c.
- [127] N. Rolston *et al.*, "Mechanical integrity of solution-processed perovskite solar cells," *Extreme Mech. Lett.*, vol. 9, pp. 353–358, Dec. 2016, doi: 10.1016/j.eml.2016.06.006.
- [128] T. J. Jacobsson, L. J. Schwan, M. Ottosson, A. Hagfeldt, and T. Edvinsson, "Determination of Thermal Expansion Coefficients and Locating the Temperature-Induced Phase Transition in Methylammonium Lead Perovskites Using X-ray Diffraction," *Inorg. Chem.*, vol. 54, no. 22, pp. 10678–10685, Nov. 2015, doi: 10.1021/acs.inorgchem.5b01481.

- [129] V. Ray *et al.*, “The impact of space weather on very low Earth orbit (VLEO) satellites,” in *Advanced Maui Optical and Space Surveillance Technologies (AMOS) Conference, 2022*. Accessed: Apr. 26, 2024. [Online]. Available: [https://amostech.com/TechnicalPapers/2022/Atmospherics\\_Space-Weather/Ray.pdf](https://amostech.com/TechnicalPapers/2022/Atmospherics_Space-Weather/Ray.pdf)
- [130] “NOAA Space Weather Scales | NOAA / NWS Space Weather Prediction Center.” Accessed: Apr. 26, 2024. [Online]. Available: <https://www.swpc.noaa.gov/noaa-scales-explanation>
- [131] “Solar Cycle 25 Is Here. NASA, NOAA Scientists Explain What That Means - NASA.” Accessed: May 06, 2024. [Online]. Available: <https://www.nasa.gov/news-release/solar-cycle-25-is-here-nasa-noaa-scientists-explain-what-that-means/>
- [132] G. Bonin, N. Orr, R. Zee, and J. Cain, “Solar array arcing mitigation for polar low-earth orbit spacecraft,” 2010, Accessed: May 06, 2024. [Online]. Available: <https://digitalcommons.usu.edu/smallsat/2010/all2010/59/>
- [133] W. Li and M. k. Hudson, “Earth’s Van Allen Radiation Belts: From Discovery to the Van Allen Probes Era,” *J. Geophys. Res. Space Phys.*, vol. 124, no. 11, pp. 8319–8351, 2019, doi: 10.1029/2018JA025940.
- [134] T. P. Dachev *et al.*, “Overview of the Liulin type instruments for space radiation measurement and their scientific results,” *Life Sci. Space Res.*, vol. 4, pp. 92–114, Jan. 2015, doi: 10.1016/j.lssr.2015.01.005.
- [135] I. Obodovskiy, “Chapter 48 - Crews and Passengers of Long-Distance Flights. Astronauts,” in *Radiation*, I. Obodovskiy, Ed., Elsevier, 2019, pp. 597–606. doi: 10.1016/B978-0-444-63979-0.00048-3.
- [136] R. B. Horne *et al.*, “Space weather impacts on satellites and forecasting the Earth’s electron radiation belts with SPACECAST,” *Space Weather*, vol. 11, no. 4, pp. 169–186, 2013, doi: 10.1002/swe.20023.
- [137] C. Nunn *et al.*, “Lunar Seismology: A Data and Instrumentation Review,” *Space Sci. Rev.*, vol. 216, no. 89, 2020, doi: 10.1007/s11214-020-00709-3.
- [138] E. Grun, “The lunar dust environment,” *Planet. Space Sci.*, vol. 59, no. 14, pp. 1672–1680, Nov. 2011, doi: 10.1016/j.pss.2011.04.005.
- [139] P. Pokorny *et al.*, “Meteoroids at the Moon: Orbital Properties, Surface Vaporization, and Impact Ejecta Production,” *J. Geophys. Res. Planets*, vol. 124, pp. 752–778, 2019, doi: 10.1029/2018JE005912.
- [140] J. H. Pomeroy and N. J. Hubbard, *The Soviet-American Conference on Cosmochemistry of the Moon and Planets: A Conference Held in Moscow, U.S.S.R., June 4-8, 1974*. Scientific and Technical Information Office, National Aeronautics and Space Administration, 1977.
- [141] G. Cremonese, P. Borin, A. Lucchetti, F. Marzari, and M. Bruno, “Micrometeoroids flux on the Moon,” *Astron. Astrophys.*, vol. 551, no. A27, 2013, doi: 10.1051/0004-6361/201220541.
- [142] J. Oberst, “Unusually High Stress Drops Associated With Shallow Moonquakes,” *J. Geophys. Res.*, vol. 92, no. B2, pp. 1397–1405, Feb. 1987, doi: 10.1029/1987JB0055891.
- [143] J.-L. Dimech, B. Knapmeyer-Endrun, D. Phillips, and R. C. Weber, “Preliminary analysis of newly recovered Apollo 17 seismic data,” *Results Phys.*, vol. 7, pp. 4457–4458, 2017, doi: 10.1016/j.rinp.2017.11.029.
- [144] Y. Liu, J. Park, E. Hill, K. D. Kihm, and L. A. Taylor, “Morphology and Physical Characteristics of Apollo 17 Dust Particles,” pp. 1–6, Apr. 2012, doi: 10.1061/40830(188)38.
- [145] N. C. Orger, J. R. Cordova Alarcon, K. Toyoda, and M. Cho, “Lunar dust lofting due to surface electric field and charging within Micro-cavities between dust grains above the terminator region,” *Adv. Space Res.*, vol. 62, no. 4, pp. 896–911, Aug. 2018, doi: 10.1016/j.asr.2018.05.027.
- [146] T. J. Stubbs, R. R. Vondrak, and W. M. Farrell, “A dynamic fountain model for lunar dust,” *Adv. Space Res.*, vol. 37, no. 1, pp. 59–66, Jan. 2006, doi: 10.1016/j.asr.2005.04.048.

- [147] A. C. Schuerger, J. E. Moores, D. J. Smith, and G. Reitz, "A Lunar Microbial Survival Model for Predicting the Forward Contamination of the Moon," *Astrobiology*, vol. 19, no. 6, pp. 730–756, Jun. 2019, doi: 10.1089/ast.2018.1952.
- [148] "Review of dust transport and mitigation technologies in lunar and Martian atmospheres - ScienceDirect." Accessed: Apr. 10, 2024. [Online]. Available: [https://www.sciencedirect.com/science/article/pii/S0273117715004111?casa\\_token=xre2jG44BpcAAAAA:CWkSWN819OEsNPmpKN2-jIHjogTQ-yOHUP85wI03drecNRCCNXr10WBoy-nviTJS09ihSWLjSQ](https://www.sciencedirect.com/science/article/pii/S0273117715004111?casa_token=xre2jG44BpcAAAAA:CWkSWN819OEsNPmpKN2-jIHjogTQ-yOHUP85wI03drecNRCCNXr10WBoy-nviTJS09ihSWLjSQ)
- [149] "Apollo 17 Lunar Surface Journal." Accessed: May 23, 2024. [Online]. Available: <https://www.nasa.gov/history/alsj/a17/a17.html>
- [150] C. M. Katzan, D. J. Brinker, and R. Kress, "The effects of lunar dust accumulation on the performance of photovoltaic arrays," Aug. 1991. Accessed: Apr. 10, 2024. [Online]. Available: <https://ntrs.nasa.gov/citations/19910020924>
- [151] A. Rahimi, O. Ejtehadi, K. H. Lee, and R. S. Myong, "Near-field plume-surface interaction and regolith erosion and dispersal during the lunar landing," *Acta Astronaut.*, vol. 175, pp. 308–326, Oct. 2020, doi: 10.1016/j.actaastro.2020.05.042.
- [152] M. X. Diaz-Lopez, M. Gorman, J. S. Rubio, and R. Ni, "Plume-surface Interaction Physics Focused Ground Test 1: Diagnostics and Preliminary Results," in *AIAA SCITECH 2022 Forum*, American Institute of Aeronautics and Astronautics. doi: 10.2514/6.2022-1810.
- [153] J. R. Gaier, "Lunar Dust 101," Nov. 18, 2008. Accessed: Apr. 10, 2024. [Online]. Available: <https://ntrs.nasa.gov/citations/20090004550>
- [154] R. Gaier, James and D. Jaworske A., "Lunar Dust on Heat Rejection System Surfaces: Problems and Prospects," presented at the Space Technology and Applications International Forum, Albuquerque, New Mexico, Feb. 2007.
- [155] P. Singh and N. M. Ravindra, "Temperature dependence of solar cell performance—an analysis," *Sol. Energy Mater. Sol. Cells*, vol. 101, pp. 36–45, Jun. 2012, doi: 10.1016/j.solmat.2012.02.019.
- [156] J. R. Gaier and M. E. Perez-Davis, "Aeolian removal of dust types from photovoltaic surfaces on Mars," 1990.
- [157] C. I. Calle, "The electrostatic environments of Mars and the Moon," *J. Phys. Conf. Ser.*, vol. 301, no. 1, p. 012006, Jun. 2011, doi: 10.1088/1742-6596/301/1/012006.
- [158] F. Forget and L. Montabone, "Atmospheric Dust on Mars: A Review," Jul. 2017, Accessed: Aug. 30, 2022. [Online]. Available: <https://ttu-ir.tdl.org/handle/2346/72982>
- [159] T. C.-J. Yang, P. Fiala, Q. Jeangros, and C. Ballif, "High-Bandgap Perovskite Materials for Multijunction Solar Cells," *Joule*, vol. 2, no. 8, pp. 1421–1436, Aug. 2018, doi: 10.1016/j.joule.2018.05.008.
- [160] M. Filipič *et al.*, "CH<sub>3</sub>NH<sub>3</sub>PbI<sub>3</sub> perovskite / silicon tandem solar cells: characterization based optical simulations," *Opt. Express*, vol. 23, no. 7, pp. A263–A278, Apr. 2015, doi: 10.1364/OE.23.00A263.
- [161] Md. R. Islam, Y. Wu, K. Liu, Z. Wang, S. Qu, and Z. Wang, "Recent Progress and Future Prospects for Light Management of All-Perovskite Tandem Solar Cells," *Adv. Mater. Interfaces*, vol. 9, no. 4, p. 2101144, 2022, doi: 10.1002/admi.202101144.
- [162] L. McMillon-Brown, T. J. Peshek, A. Pal, and J. McNatt, "A study of photovoltaic degradation modes due to dust interaction on Mars," *Sol. Energy Mater. Sol. Cells*, vol. 221, p. 110880, Mar. 2021, doi: 10.1016/j.solmat.2020.110880.
- [163] J. Appelbaum and D. J. Flood, "Solar radiation on Mars," *Sol. Energy*, vol. 45, no. 6, pp. 353–363, 1990, doi: 10.1016/0038-092X(90)90156-7.
- [164] G. A. Landis, K. Herkenhoff, R. Greeley, S. Thompson, P. Whelley, and Mer Athena Science Team, "Dust and Sand Deposition on the MER Solar Arrays as Viewed by the Microscopic Imager," p. 1932, Mar. 2006.

- [165] C. S. Cockell, "The Ultraviolet Radiation Environment of Earth and Mars: Past and Present," in *Astrobiology: The Quest for the Conditions of Life*, G. Horneck and C. Baumstark-Khan, Eds., Berlin, Heidelberg: Springer, 2002, pp. 219–232. doi: 10.1007/978-3-642-59381-9\_15.
- [166] O. Melnik and M. Parrot, "Electrostatic discharge in Martian dust storms," *J. Geophys. Res. Space Phys.*, vol. 103, no. A12, p. 29107, Dec. 1998, doi: 10.1029/98JA01954.
- [167] A. Fabian, C. Krauss, A. Sickafoose, M. Horanyi, and S. Robertson, "Measurements of electrical discharges in Martian regolith simulant," *IEEE Trans. Plasma Sci.*, vol. 29, no. 2, pp. 288–291, Apr. 2001, doi: 10.1109/27.923710.
- [168] "Modeling the formation of electrostatic discharges on Mars - Krauss - 2006 - Journal of Geophysical Research: Planets - Wiley Online Library." Accessed: Jul. 02, 2024. [Online]. Available: <https://agupubs.onlinelibrary.wiley.com/doi/full/10.1029/2004JE002313>
- [169] C. I. Calle *et al.*, "Electrodynamic Shield to Remove Dust from Solar Panels on Mars," p. 5.
- [170] S. J. Bolton *et al.*, "Jupiter's interior and deep atmosphere: The initial pole-to-pole passes with the Juno spacecraft," *Science*, vol. 356, no. 6340, pp. 821–825, May 2017, doi: 10.1126/science.aal2108.
- [171] "Solar System Exploration - NASA Science." Accessed: Nov. 21, 2024. [Online]. Available: <https://science.nasa.gov/solar-system/>

## Highlights

- Space environments are surveyed with respect to perovskite-based photovoltaic performance.
- Thermal, radiation, vacuum, gaseous, and other space stressors are discussed.
- General testing needs for perovskite-based photovoltaics are detailed.

Journal Pre-proof

**Declaration of interests**

The authors declare that they have no known competing financial interests or personal relationships that could have appeared to influence the work reported in this paper.

The author is an Editorial Board Member/Editor-in-Chief/Associate Editor/Guest Editor for *[Journal name]* and was not involved in the editorial review or the decision to publish this article.

The authors declare the following financial interests/personal relationships which may be considered as potential competing interests: